3.7 Effect of parameter changes (b): Robustness

The describing function analysis can also be used to examine the robustness of the oscillators. Robustness in this context means either that the coupled system has the same performance or behavior over a wide range of oscillator parameters, or that given a single set of parameters, a wide range of system properties give the same behavior. The oscillators are robust in both senses of the word. The oscillator parameters are generally well-behaved, with a smooth monotonic effect on the system behavior, decoupled from the effects of the other parameters.

Robust properties greatly ease the implementation of oscillator driven systems since very little tuning is required to achieve good results. This section evaluates each of the oscillator parameters in turn.

Input gains and tonics. The tonic parameter c affects the output amplitude of the oscillator and is effectively decoupled from the all the other parameters. The output amplitude is independent of input size and frequency (as shown in figure 3-7). This independence is a consequence of the non-linearities on the input g in equations (3.1) and (3.3). Appendix C shows that without these non-linear terms the system output is a function of input size, and is less well-behaved. The effect of the tonic parameter is monotonic, as was shown in figure 3-2.

The input parameter h is also decoupled from the oscillator parameters which set frequency. It has a more interesting effect on the overall system properties. In practice, the parameter does not have much effect on the final motion. It needs to be large enough to cause entrainment, but other than that its value is unimportant. The reason for this can be seen in figure 3-13, which plots the describing function for the oscillator with two different values of input gain. The two different solutions are $\omega_f = 8.82, A_f = 0.38$ for $h = 0.7$, and $\omega_f = 8.98, A_f = 0.77$, for $h = 1.7$. In spite of the gain more than doubling, the frequency changes by less than 2%. Since A_f is the amplitude of input to the oscillator, the actual motion has amplitude A_f/h, which is 0.55 when $h = 0.7$, and 0.45 when $h = 1.7$, a change of about 15%. Looking at figure 3-13, the reason for this robustness is the approximately radial lines of the oscillator describing function, particularly in the middle frequencies. The oscillator is inherently robust to changes in input size, giving approximately the same performance for a wide variety of parameter values.

For a fixed set of gains, the range of phases, frequencies, and gains that the oscillator can produce is large, so that any part of the system phase plot which overlaps with the area covered by the oscillator will produce an oscillatory solution. This contributes to the robustness of the oscillator itself.

Time constants. The main effect of changing the time constants of the oscillator is to change the frequency range of the oscillator. This effect is monotonic, as shown clearly in figure 3-2. As mentioned above, the effect is decoupled from the input gain and tonic parameters.

Referring to figure 3-13, if the lines were radial, then the effect of changing the time constants would be a monotonic change in the frequency of the coupled system. The lines are not exactly radial, which gives rise to the resonance tuning behavior of the system. The oscillator can tune into the resonant frequency of a driven system for a wide range of oscillator parameters, and conversely, for a fixed set of oscillator parameters, can tune into the frequency of a range of systems.

Figure 3-14 shows the range of settings of input gain and time constant which have a final solution which is within 10% of the system natural frequency. The plot shows that the oscillator natural frequency can vary from 3.5–5.5 rad/s which is a percentage change of 40 %, and the gain can vary even more (from 0.2 to 2), while still finding the resonant frequency. This was for a simulated system with $k = 20, m = 0.4, b = 5.2$.

Taking parameters for the oscillator in the middle of these values, i.e. $w_n = 4.5, h = 1$, the robustness of the oscillator to changing systems can be measured. The stiffness can be varied from 14–25.4 Nm/rad with the final frequency remaining within 10% of the natural frequency. This is a

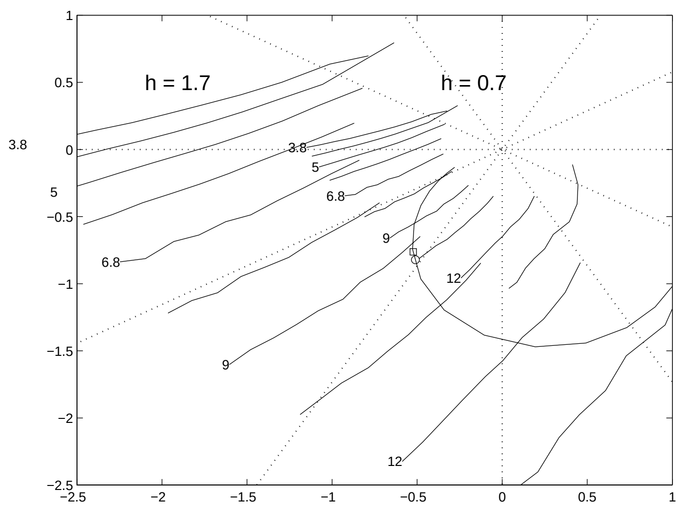

Figure 3-13: $\boxed{\text{SIM}}$ Figure showing the effect of the gain on the describing function of the oscillator. The plot shows $1/N(j\omega, A)$ plotted on the complex plane for two values of input gain h, as marked. It also shows $G(j\omega)$ for a typical mass-spring system, with the limit cycles marked with a $\circ$ for $h = 0.7$, and a $\Box$ for $h = 1.7$. Because the lines of $1/N$ are approximately radial (especially for the middle frequencies), the effect of doubling the gain on the coupled system behavior is small. For high and low frequencies, changing the gain will alter how the oscillator couples with another system but the effect of the gain is still minor, given the acute angles between the lines and the radial directions.

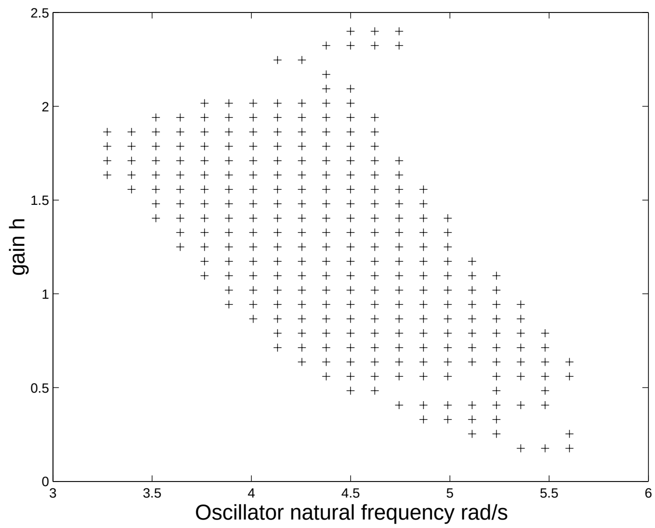

Figure 3-14: $\boxed{\text{SIM}}$ Figure showing the range of values of the oscillator natural frequency, and oscillator input gain over which the final frequency of a coupled oscillator, mass-spring system was within 10% of the system natural frequency. The mass-spring system had values $k = 20, m = 0.4, b = 5.2$ corresponding to a natural frequency of 8.66 rad/s and damping ratio of 0.3.

30% change in stiffness, or approximately a 12% change in system resonant frequency. These results demonstrate clearly the robustness of the oscillator to parameter values and to changes in the system properties.

This resonance tuning behavior is the natural behavior of the coupled system. Since the oscillators entrain quickly, this means that the oscillator system is reactive to fast changes in the dynamics. An alternative method would be to identify the system and use a constant frequency command to excite the resonant frequency. While this method would probably give more accurate resonant tuning, it would not be responsive to changes in the dynamics without re-identifying the system.

The resonant frequency is also the most efficient speed to move the mass-spring system, with the minimum of real work required to produce the motion. The fact that the oscillator can find and drive at this frequency, while still adapting to the system properties is thus a useful behavior.

System changes The oscillator is also robust to other changes in the system properties. For example, changing the damping in the system alters the shape of $G(j\omega)$, but does not alter the frequency. Since the oscillator can produce a variety of gains and frequencies, it is automatically robust to these changes. For example, the damping ratio of the example system described above can be altered from 0.12 to 0.5 while still remaining entrained, with the entrained frequency varying from 7.56 to 6.59 rad/s where the resonant frequency is 7.07 rad/s, as shown in figure 3-15. This corresponds to a 7% change in frequency.

Entrainment The final aspect of the oscillator control which is practically useful is that it tends to entrain very quickly, usually within one cycle. This means that it is easy to tell whether a parameter is correct or not as the system settles quickly. This is also improves the robustness, since the oscillator responds quickly to changes in the dynamics.

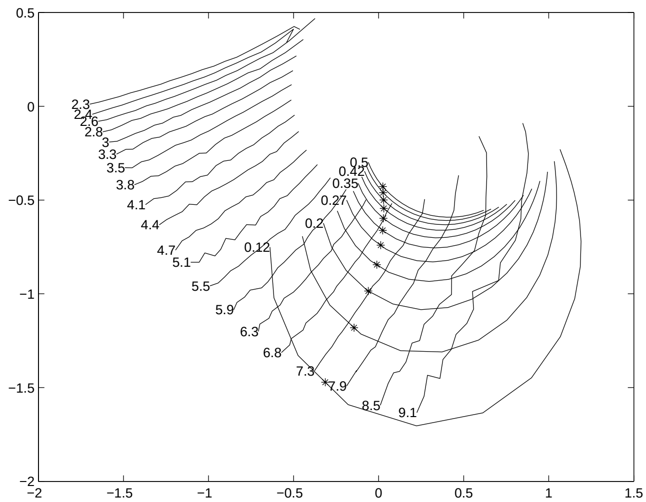

Figure 3-15: $\boxed{\text{SIM}}$ Figure showing the effect of varying the damping ratio of the mass-spring system. The plot shows the describing function for the oscillator with lines for $G(j\omega)$ for different values of the damping ratio as marked. The damping ratio can be altered from 0.12 to 0.5 while remaining entrained, with only a 7% change in the output frequency away from the resonant frequency: frequency varies 7.56–6.69 rad/s, with the resonant frequency of 7.07 rad/s.

3.8 Design example: Resonance tuning

The describing function analysis is not only appropriate for analyzing the Matsuoka oscillator. This section shows how it can be used to analyze the well known Van der Pol oscillator, for the task of resonance tuning. There have been a number of papers concerning the resonance tuning property of neural oscillators (e.g. Hatsopoulos et al. (1992), Hatsopoulos and Warren (1996), Epstein and Kopell (1999)), without any full explanation of why this behavior is observed or predictions of its limits. The describing function analysis provides answers to both of those questions.

The Van der Pol (VDP) oscillator (Strogatz, 1994, p. 198), is described by the following equations:

$$\tau \dot{u} = wv + f(u) + h_j g_j \tag{3.13}$$

$$\tau \dot{v} = -\epsilon u \tag{3.14}$$

$$f(u) = u - u^3/3 \tag{3.15}$$

$$y_{out} = h_o u \tag{3.16}$$

where u and v are state variables, g_j is an input, h_j a gain on the input, h_o is a gain on the output, τ determines the speed of the oscillator, and ϵ is a parameter.[4]

The describing function for this oscillator is illustrated in 3-16, which shows a rather different pattern from the Matsuoka oscillator. The same trends are evident; the gain reduces with increasing A, although the output amplitude alters as a function of A, making the range of gains less uniform. The gain as before is roughly constant with frequency. The phase is roughly independent of amplitude, in the range $\pm 30°$.

[4]Reasonable values are $0.1 \le \epsilon \le 0.1, 1 \le h_j \le 30, 0.1 \le h_o \le 1$.

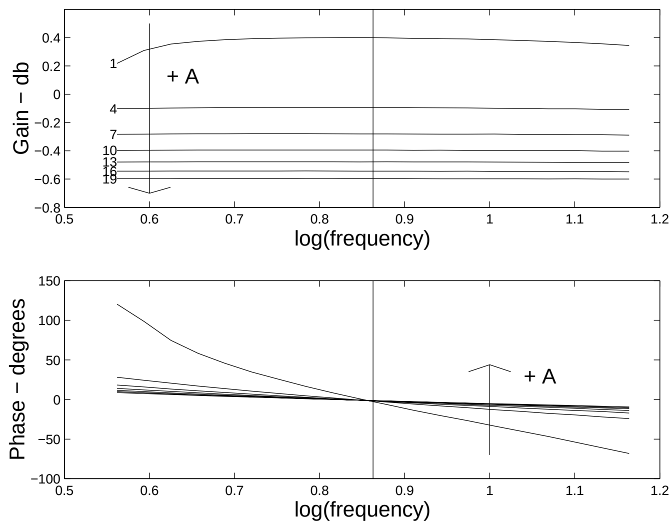

Figure 3-16: $\boxed{\text{SIM}}$ Van der Pol Bode plot. The top graph shows the gain $|N(j\omega, A)|$ plotted against frequency, and the lower plot the phase. The multiple lines correspond to different values of input amplitude A as indicated by the numbers and arrows on the plot. The gain is inversely related to A and is roughly constant with frequency. Unlike the Matsuoka oscillator, the output amplitude of the VDP oscillator is a function of the input amplitude. This results in the lines in the gain plot not being equally spaced (compare to figure 3-7). The phase is less dependent on A, and is grouped around zero degrees. The natural frequency of the oscillator is indicated by the vertical line.

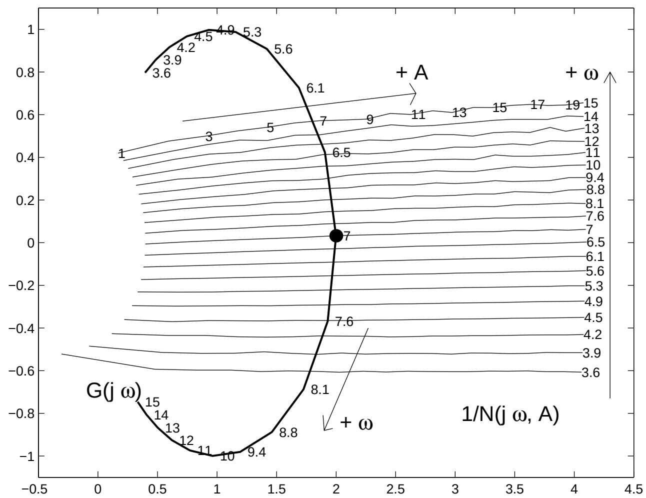

Figure 3-17: $\boxed{\text{SIM}}$ Plot of $G(j\omega)$ and $1/N(j\omega, A)$ in the complex plane for the VDP oscillator. $G(j\omega)$ is the thick line, with numbers indicating frequency. The lines for $1/N(j\omega, A)$ correspond to constant frequency, with amplitude A increasing along each line as indicated by the numbers and arrow. There is a limit cycle solution at the point where the two graphs intersect at the same frequency. The intersection point is indicated by a filled circle, at $\omega = 7.0$ and $A = 7.4$. This plot was produced for $\tau_1 = 0.03, \epsilon = 0.1, h_o = 0.2, h_j = 1, k = 20, m = 0.4, b = 2$.

If this oscillator is connected to a mass-spring system as before, because the Van der Pol oscillator can only produce phases in the range $\pm 30°$, the intersections would all be at low frequencies. However, if the velocity rather than the position is used as input, those phases correspond to points near the resonant frequency of the system. This is illustrated in figure 3-17, which shows $G(j\omega)$ for a mass-spring system with input θ_v, and output velocity $\dot{\theta}$, plotted together with $1/N(j\omega, A)$. The input and output gains are calculated to position the two plots over one another, here $h_j = 1, h_o = 0.2$. As before, there are limit cycle solutions where the graphs intersect at the same frequency, here $\omega = 7.0, A = 7.4$.

Because of the shape of the phase plot of the VDP, the oscillator can tune into the resonant frequency of the plant motion over a range of system frequencies. The Matsuoka oscillator also has this effect, but because the lines of its describing function are not as parallel, or as aligned with the resonant phase difference as the VDP characteristic, the resonance tuning behavior is not as strong. Using the describing function analysis, the resonance tuning effect of the VDP can be calculated, and measured in simulation. Figure 3-18 shows the result of this prediction. The plot shows the oscillator tuning into the resonant frequency of the system over a large range of frequencies. The accuracy of the describing function prediction is also shown in the graph.

To confirm this result, the VDP oscillator was implemented on the robot, and a similar experiment was conducted, varying the stiffness of a robot joint, and measuring the final frequency. The results from this are plotted in figure 3-19. The results show that over a range of frequencies corresponding to a four-fold increase in stiffness, the VDP oscillator drove the system at its resonant frequency.

This example illustrated not only the performance of the VDP oscillator system in this task, but also the use of describing function analysis to design and predict final system performance.

The VDP oscillator is in general less robust than the Matsuoka oscillator. This is because the

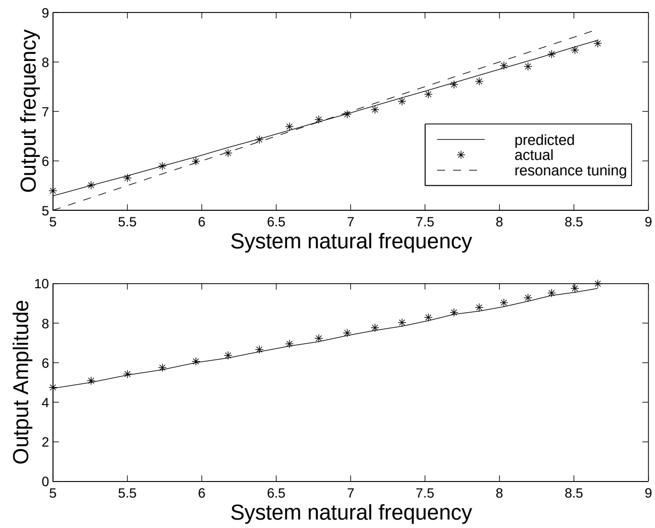

Figure 3-18: $\boxed{\text{SIM}}$ Prediction of VDP oscillator driving a mass, using velocity as the oscillator input. The upper plot shows the accuracy of the prediction, and the resonance tuning behavior of the oscillator. The oscillator drives the mass at the resonant frequency of the mass-spring system, over a range of different conditions (here the frequency of the mass-spring system is varying from 5 to 9 rad/s). The lower plot shows the accuracy of the prediction of motion amplitude. For these plots $\tau_1 = 0.03, \epsilon = 0.1, h_o = 0.1, h_j = 2, k = 20, m = 0.4, b = 2$.

output amplitude is dependent on the input amplitude, making tuning difficult, and because the range of output phases is much less.

3.9 Design example: Juggling

This section describes the application of describing function analysis to a more complex task, that of juggling a ball on a paddle. The setup is illustrated in figure 3-20. This task has been addressed by a number of researchers, (Schaal and Atkeson, 1993, Rizzi and Koditschek, 1994), including one using neural oscillators (Miyakoshi et al., 1994). Using the method presented in this chapter, not only can the parameters be easily tuned without intensive simulation, but the robustness of the system can be calculated and compared to other approaches.

Schaal and Atkeson (1993) showed that when juggling a ball on a paddle, stable motion is achieved when there is a particular constant phase difference between the paddle and ball motion. This motivates the approach of writing the juggling problem as a describing function, where stable juggling is defined in terms of a phase between input (paddle motion) and output (ball motion), as well as a gain (the amplitude of the ball). Although this is a rough approximation to juggling, it allows analysis of the situation. The setup is shown in figure 3-21, where the paddle is assumed to move sinusoidally, i.e. $y(t) = B\sin(\omega t)$, and the ball bounces with height x. Since the juggling is stable, the velocity of the ball before and after impact is the same, so the impact equation is

$$(\dot{x} - \dot{y}) = -\alpha(-\dot{x} - \dot{y}) \tag{3.17}$$

where α is the coefficient of restitution. Calculating the time between bounces (which is $2\pi/\omega$), and

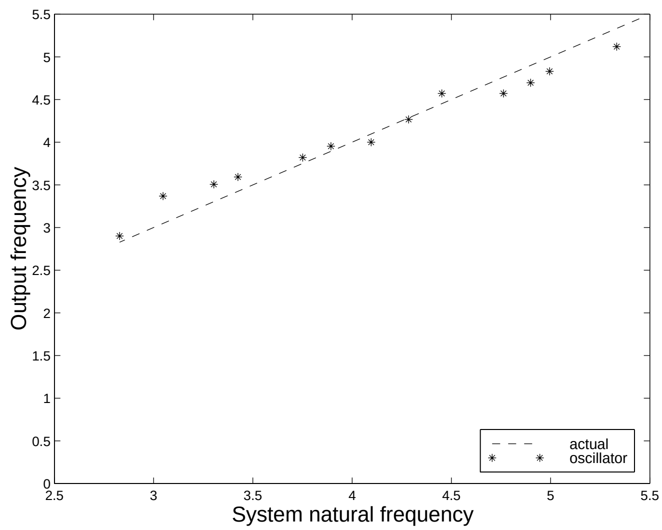

Figure 3-19: REAL Plot shows resonance tuning action of a VDP oscillator actuating a joint on the real robot. The stars mark measured frequency, plotted against the natural frequency of the system (also measured), as the stiffness of the system was altered. The results fit with the predictions of the describing function analysis. Because the natural frequency is a function of the square root of the system stiffness, the actual stiffness varied from 9 to 42.

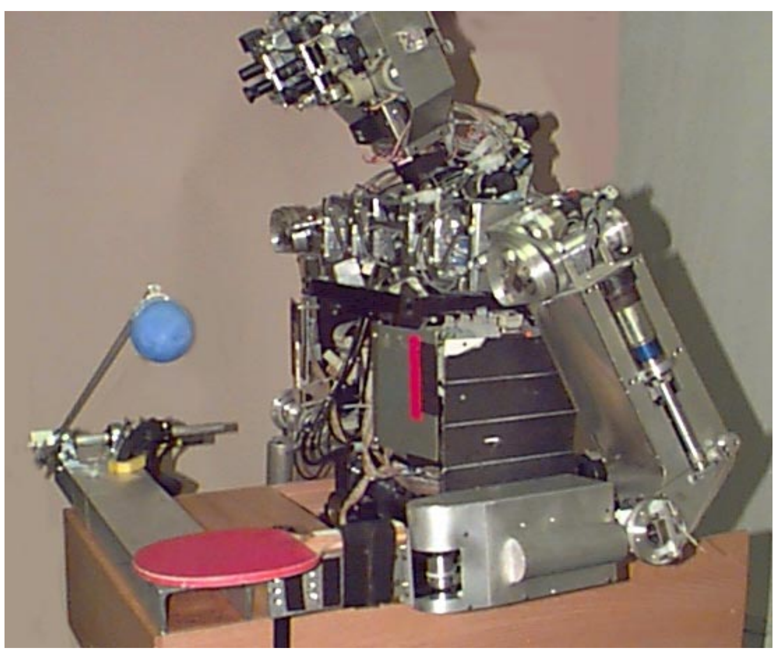

Figure 3-20: Picture of robot in juggling task. The paddle is a table tennis bat attached to the robot's arm. The ball is restrained to travel in one dimension by being mounted on a rotating boom. The angle of the boom is measured using a potentiometer at the pivot point, and this feedback signal is used by the oscillator to coordinate the arm motion with the ball motion.

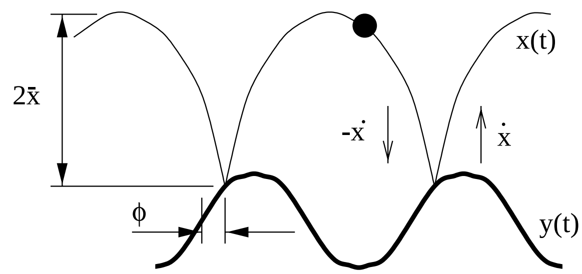

Figure 3-21: Schematic of the juggling action. The thick line shows the motion of the paddle $y(t) = B\sin(\omega t)$, and the thin line the ball trajectory $x(t)$. The ball impacts the paddle at a phase ϕ of the sine wave. The analysis expresses the juggling as a describing function, writing a stable solution in terms of the phase difference between ball and paddle trajectories $(\phi + \pi/2)$, and the amplitude of the ball motion $\overline{x}$.

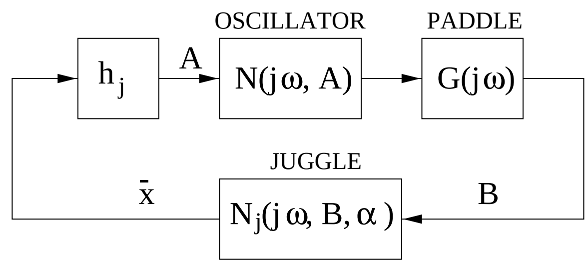

Figure 3-22: Oscillator driven juggling. The amplitude of the ball motion is $\overline{x}$, the input to the oscillator is $A = h_j\overline{x}$, and the output of the oscillator drives the paddle ($G(j\omega)$) with amplitude B. The ball motion can then be calculated using N_j. As before, there can be only a limit cycle when the loop gain is unity.

substituting $\dot{y} = B\omega\cos(\phi)$ at impact gives an equation for the phase at impact:

$$\phi = \arccos\left[\frac{\pi g}{B\omega^2}\left(\frac{1-\alpha}{1+\alpha}\right)\right] \tag{3.18}$$

Calculating the maximum height of the ball (at the time halfway between bounces) gives an expression for the ball amplitude:

$$\overline{x} = g\pi^2/4\omega^2 \tag{3.19}$$

This makes the describing function for the juggling $N_j(j\omega, B, \alpha) = \overline{x}\exp(-j(\phi + \pi/2))$. The paddle is driven by an oscillator with the same control system as before, i.e. through a spring, so that the oscillator output drives the desired position of the paddle, and the input is the ball trajectory x, as illustrated in figure 3-22. Since the juggle describing function is a non-linear function of B, which is itself generated by the non-linear oscillator/paddle, the functions cannot be separated and plotted as before. A loop gain, and a condition for stable oscillator driven juggling can still be calculated:

$$\overline{x} = N_j(j\omega, [h_j\overline{x}N(j\omega, h_j\overline{x})G(j\omega)], \alpha) \tag{3.20}$$

This can be solved numerically for the values of A, and ω which give stable juggling given the other parameters $(h_j, A_n, k, m$ etc.).

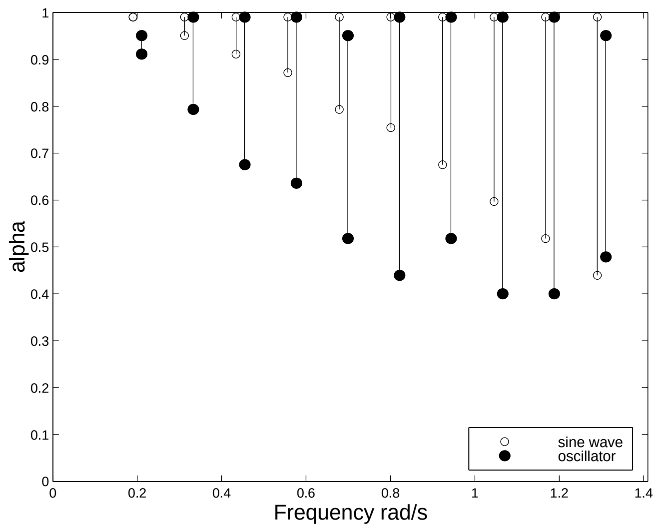

Figure 3-23: $\boxed{\text{SIM}}$ Robustness to changes in α. The plot shows ranges of α for which stable juggling can be achieved by either an oscillator with natural frequency ω_n, ($\bullet$), or a constant frequency sine wave $B\sin(\omega_n t)$, ($\circ$), as the frequency ω_n is varied. Because the oscillator can alter its frequency, it is more robust to changes in α than the constant frequency solution, and thus more suitable for the task.

Solving this equation is a powerful tuning tool. Using the equation, it was found that using ball velocity $\dot{x}$ rather than the ball trajectory x as input gave more robust solutions. This would have been very difficult to discover without this analysis.

Solving this equation is also powerful for measuring robustness and comparing solutions. The robustness of the oscillator solution can be measured by fixing the oscillator parameters and calculating whether solutions exist for different values of restitution coefficient α. This can be compared to a similar calculation for a constant sine wave $y(t) = B\sin(\omega t)$. For the sine wave, the limit on α is given by real solutions of equation (3.18). The maximum value of α is 1, and the minimum is a function of frequency:

$$\alpha_{min} = \min(0, (1 - B\omega^2/g\pi)/(1 + B\omega^2/g\pi)) \tag{3.21}$$

Figure 3-23 shows the comparison between oscillators with natural frequency ω_n against sine waves of frequency ω_n, over a range of different ω_n's. The oscillators use velocity as input. The lines on the graph show the range of α's over which the different methods could stably juggle. Because the oscillator can produce outputs over a range of frequencies, it can juggle with a wider range of α's than the constant frequency solution. This result shows that oscillators are a better solution than a constant sine wave for this task.

Motivated by these results, juggling was implemented using a paddle attached to the arm of the robot. The setup is shown in figure 3-20. The ball was restricted to move in one dimension by a lightweight boom whose angle was measured using a potentiometer. As indicated by the analysis, ball velocity was chosen as the input signal to the oscillator. Figure 3-24 shows a short transient from the juggling performance. The juggling is much more variable than a simulated version, since there is a great deal of noise not only in the sensor signal, but also in the way the robot hits the tethered ball, effectively altering α for each impact. The change in speed of the oscillator driven paddle is visible in the plot. The oscillator responds on a hit by hit basis, remaining coordinated

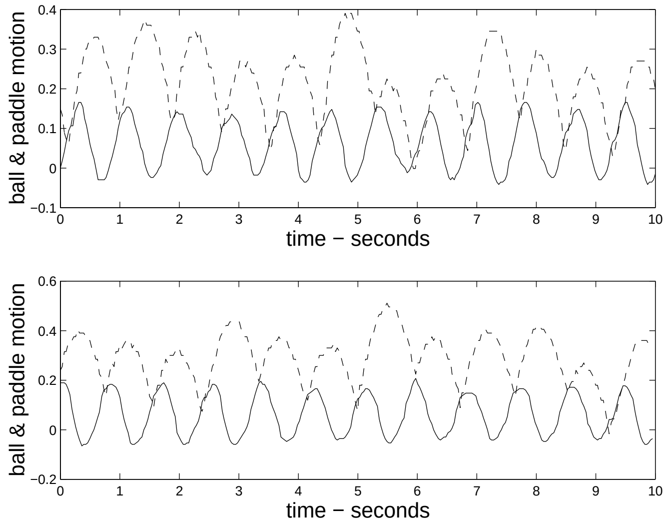

Figure 3-24: REAL Plot showing paddle position (solid) and ball trajectory (dashed) against time for 2 traces of the robot juggling. Because of the way the arm hits the ball, there is significant noise in the system. The oscillator responds to the changing amplitude of the ball by adjusting its speed slightly, which is noticeable in the middle of the trace.

with the ball motion.

3.10 Adaptation

As well as responding to the type of system, and adjusting its frequency with respect to the system properties, the oscillator synchronizes itself with the mass motion. This was seen in the juggling example, the oscillator coordinating the motion of the paddle with the height of the ball on a hit by hit basis. The same action occurs when driving a single robot joint. This is because the oscillator is tightly coupled, and the oscillator output is referenced relative to its input, which is the motion of the joint. This means that the oscillator is sensitive to changes in the motion of the joint. For example if the oscillator is moving a certain link back and forth, and something or someone moves the link, the oscillator entrains with the imposed motion, and remains synchronized. This is illustrated in figure 3-25. The oscillator is sensitive to the exact motion of the joints, and not just the general system properties. This behavior and sensitivity is important and useful for providing coordination between the joints through the natural dynamics. This topic is examined in more detail in chapter 4.

3.11 Conclusion

This chapter has introduced the oscillators, and described their behavior coupled to single degree of freedom mechanical systems. Analysis using describing functions was introduced, and was shown to be powerful for analyzing the motion, predicting the behavior of the coupled system, and a practical tool for tuning, evaluating the robustness of the parameters, and evaluating the oscillator approach.

Using this analysis on oscillators reveals some general principles which apply to the oscillator solutions.

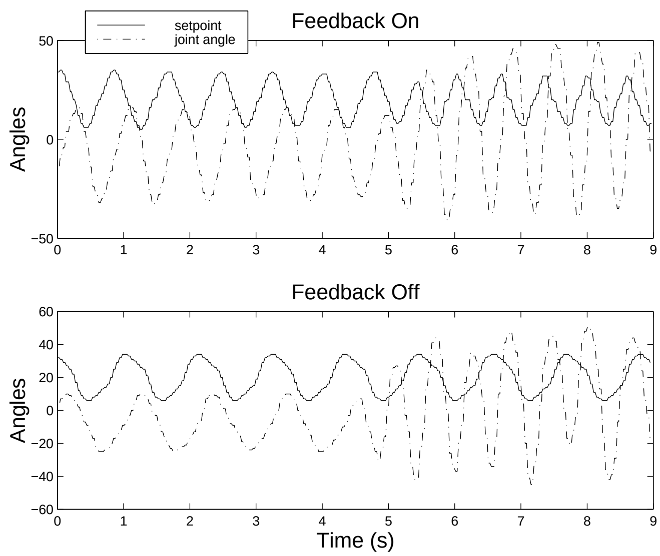

Figure 3-25: REAL Effect of external disturbances on the oscillator entrainment. The plots show the oscillator outputs (solid) and the joint angle (dash dot) for a single joint of the robot. Approximately halfway through the trace, the arm was moved by the author at a higher frequency and larger amplitude. When feedback is used (top graph), the oscillator responds to the extra motion, and remains entrained, its output tracking the imposed motion. In the lower trace when the feedback is off, the oscillator ignores the imposed motion, which is thus more jerky, since the oscillator and the disturbance are not coordinated.

- Robustness in parameter settings. Due to the wide range of gains that the oscillator can produce, the oscillator will entrain with a wide range of different systems. The behavior of the oscillator also makes the parameters of the oscillator robust because changing them either has a minor, or a predictable effect. The effect of varying parameters is smooth, monotonic, and they are decoupled from one another. This has the consequence that the system is easy to use in practice, it being easy to choose working parameters.

- Sensitivity to system changes. Again due to the shape of N, oscillator systems are sensitive to changes in the resonant frequencies of the mechanical systems, driving them at frequencies close to the resonant frequency. This occurs over a wide range of oscillator parameters, and a range of system frequencies. The oscillator behavior is automatic and is reactive, altering quickly when the system dynamics change. Since the resonant frequency is an efficient speed to move a mass-spring system, the oscillator behavior is finding the best speed, dependent on the natural dynamics.

- Stability of final solutions. Due to the shape of the plots, the oscillators produce stable motions actuating common mass-spring mechanical systems. This together with their observed fast entrainment to limit cycle solutions makes them well suited for practical applications.

- Synchronization. The oscillator produces a command to the joints which is defined relative to the joint motion. The oscillator is thus sensitive and responds to the joint motion, driving slower or faster when the joint is forced by the system, be it another joint of the arm or a human grabbing and moving the arm. This adaptation is crucial to the oscillator behavior when driving multiple degrees of freedom, as described in the following chapter.

Chapter 4

Coupling through natural dynamics

This chapter examines the behavior of the oscillators while driving multiple degrees of freedom of the arm, as opposed to the single degree of freedom motions examined in the previous chapter. The oscillators are connected to drive each joint of the arm independently, as shown in figure 4-1. There is a tightly coupled oscillator at each joint, with no connections between them. The oscillators use mechanical coupling through the physical arm to coordinate with one another and the task.

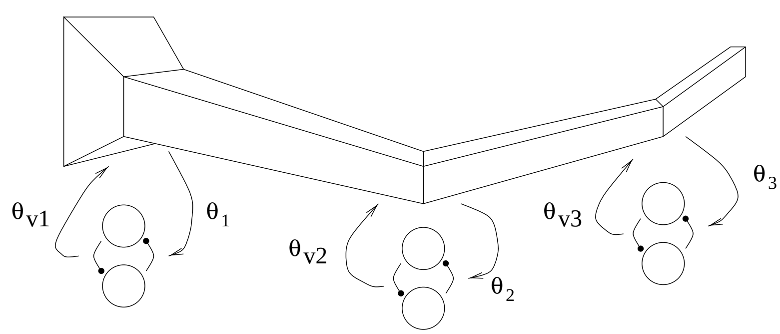

Figure 4-1: Figure showing configuration of oscillators and arm throughout this chapter. The oscillators are tightly coupled to each joint, with their output driving the setpoint θ_{vi}, and their input being either the joint angle θ_i, or the joint torque u_i. There are no software connections between the oscillators; they use mechanical coupling through the physical arm detected using the feedback to coordinate with one another and the task.

The versatility of this configuration is demonstrated using a number of examples, including crank turning using both one and two arms, and with the arms in both redundant and non-redundant configurations. Other position constrained tasks such as pumping a bicycle pump have also been demonstrated. The configuration can also exploit the dynamics of objects for coordination of the joints; the chapter includes the example of two arms coordinated through the dynamics of a Slinky toy, which is passed from hand to hand.

The analysis tools introduced in chapter 3 are extended to analyze these multi-degree of freedom motions. The analysis indicates again the sensitivity of the oscillators, showing that their behavior is to drive the resonant mode of the mechanical system. This is appropriate for a range of tasks, for example, attaching a crank to the arm creates a low frequency resonant mode of the system, which the oscillators automatically find and drive.

The crank turning example is analyzed in the context of these results, showing also the robustness of the oscillator solutions, with many different parameter settings giving crank turning, and a single set of oscillator parameters being robust to large changes in the arm dynamics.

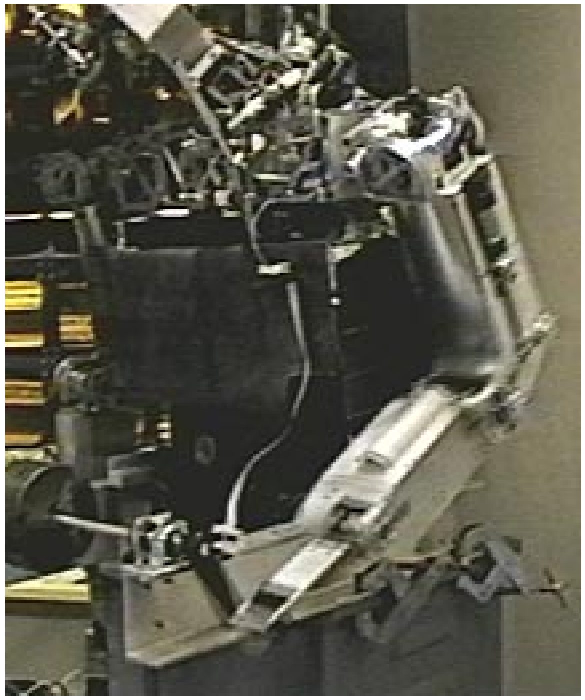

Figure 4-2: $\boxed{\text{REAL}}$ Crank turning with one arm. The picture shows the robot using its left arm to turn the crank. Oscillators are used at the shoulder and elbow in this configuration. The oscillators are initially uncoordinated, but use feedback from the motion of the joints to adjust their outputs, so turning the crank.

The chapter as a whole points out the self-organizing property of the oscillators, performing complex mechanical tasks which require coordination between the joints in a simple and robust manner.

4.1 Examples

The first example is crank turning. The oscillators have been used to turn cranks in a variety of different configurations, the most simple of which is shown in figure 4-2. Here two oscillators driving the shoulder and elbow joints are used to turn the crank in the plane. They use feedback of the joint angle to modify their outputs. As described above, there is no explicit connection between the oscillators at the two joints, their only connection being through the mechanics of the arm, and their feedback.

When the feedback is off, the oscillators oscillate at their natural frequencies, producing uncoordinated rhythmic drives to the arm joints. When the feedback is switched on, the oscillators respond to the dynamics of the situation, become coordinated with one another, and turn the crank smoothly, as shown in the transients in figure 4-3. Because the oscillators entrain rapidly, the crank turning settles down rapidly to a steady motion. The crank turning behavior is robust to changes in most of the oscillator parameters (gains, time constants etc), and is sensitive more to the posture of the arm, and the sizes of the oscillator amplitudes (tonic). The posture and the amplitudes determine whether the arm goes all the way round, and whether the final motion is smooth and energy efficient, or more violent. Because the arm is compliant, the system is still fairly robust to these values, with a variety of postures and amplitudes giving crank turning motion. This is considered

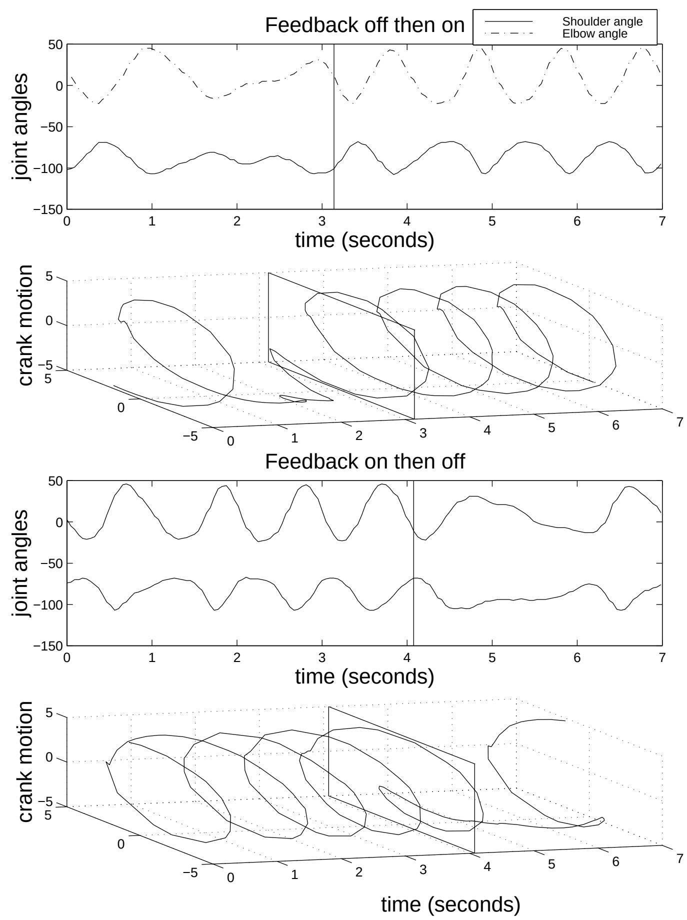

Figure 4-3: $\boxed{\text{REAL}}$ Figure showing the effect of feedback for crank turning using two degrees of freedom in the configuration shown in figure 4-2. The lines show the angles of the joints. When the feedback is on, the oscillators are coordinated with one another, and the crank is turned (the crank angle is the dash-dot line, which wraps around at 180 degrees). Without feedback the oscillators revert to their natural frequencies, which does not result in smooth crank turning. The glitch in the crank trace is caused by the angle sensor wrapping round, not by a jerk in the motion.

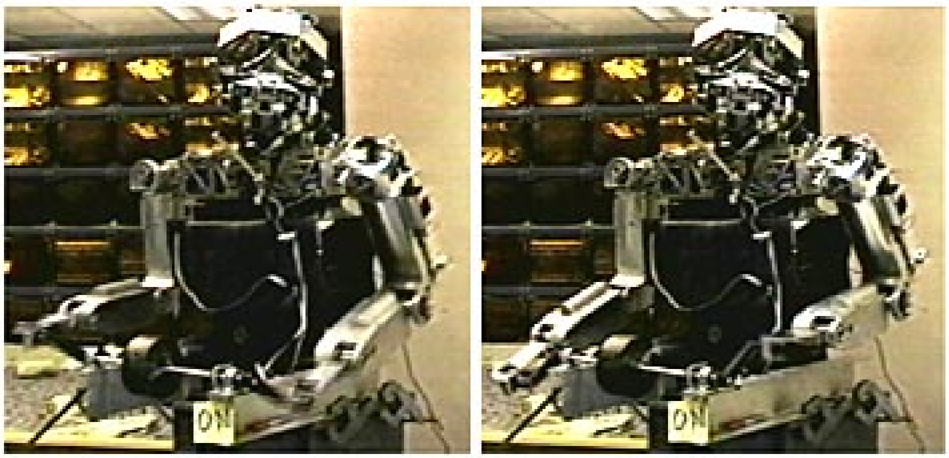

Figure 4-4: $\boxed{\text{REAL}}$ Crank turning with more than one arm. Since the oscillators are independent, the crank turning can be easily extended to use more than one arm. Here two arms are used to turn the crank, using four oscillators with two on each arm. As before, the oscillators are synchronized through mechanical coupling, there being no explicit connections between the oscillators on a single arm, or between the two arms.

in detail in section 4.7.

Since the control of the joints is independent, it makes no difference whether one or two arms are used. Figure 4-4 shows two arms turning the crank where each arm is in the same configuration as before. Four oscillators are used to achieve the motion, driving both shoulders and both elbows.

The crank is connected to the arm, and thus provides a strong constraint on how the arm can move. This is particularly the case in the configurations shown in figures 4-2 and 4-4 because the arm is not in a redundant configuration.[1] The motion of the crank determines how the shoulder and elbow joints can move. Because the oscillators use feedback from the joint angle, and because they provide an output which is a certain phase difference from their input signal (as described in chapter 3), they respond to the constraint by driving the arm around it.

The oscillators can also find crank turning solutions when the arm is redundant, i.e. configurations where the crank does not completely specify how the joints should move. A redundant configuration is shown in figure 4-5, where between four and six degrees of freedom can be used to turn the crank. The turning in this redundant case has the same properties as the non-redundant configurations: coordination through mechanical coupling, quick entrainment (see figure 4-6), and robustness to parameter changes. The oscillators have also been used for other constrained tasks such as pumping a bicycle pump.

Since the oscillator outputs are approximately sinusoidal, and the joint angle motions induced by the constraint are not sinusoidal (as in figure 4-6), there is a considerable tracking error. If the arm were stiff, this would be a problem and might cause the arm to jam. However, because the arm is compliant, the error is absorbed in the arm compliance, and the final motion is smooth. The compliance of the arm thus gives robustness. In addition, the compliance together with the position constraint expands the repertoire of the oscillators. The system exploits the crank itself to create a motion which is not solely created by rhythmic commands at the joints.

There have been many robotic approaches to crank turning, for example using impedance control

[1]There are actually three joints in the plane of the arm, the shoulder, elbow and wrist, which makes this configuration redundant. However, the wrist joint was not actuated and maintained a constant stiffness, so to all intents and purposes the configuration is not redundant.

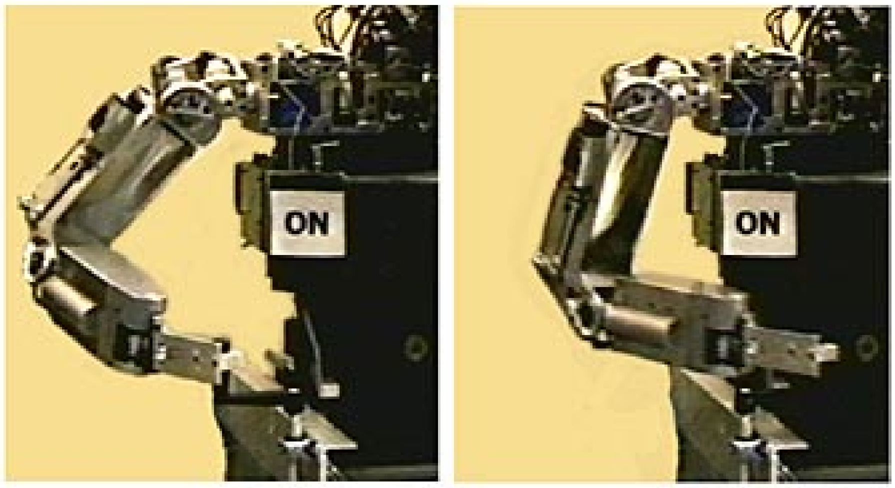

Figure 4-5: $\boxed{\text{REAL}}$ Crank turning using a redundant arm. The oscillators can be used to turn cranks even when the arm is redundant, as shown here. The arm uses 4 oscillators, driving 4 degrees of freedom, two in the shoulder, and two in the elbow. The transients from this system are shown in figure 4-6.

(Hogan, 1985a), or hybrid force/position control (Raibert and Craig, 1981). These approaches use knowledge about the arm and crank kinematics to both move the arm to the crank, and to coordinate multiple degrees of freedom to turn the crank. They use this kinematic knowledge to deal with cranks of different sizes and different locations. The oscillator solution requires no calibration or kinematic transformations, but is only solving half of the problem. The arm starts connected to the crank, the posture and oscillator amplitudes set for the particular crank size and position, and the oscillators only provide the coordination for the motion. Even for creating the motion, the oscillator solution is more simple, with uncalibrated identical local controllers interacting through the arm mechanics, compared to a single complex calibrated kinematic controller.

The reason why the local control works is that the arm is compliant, making the interaction with the crank robust and giving some dynamics to exploit, and that the oscillators have the right properties to be local controllers for these tasks. These properties are examined later in this chapter.

Even in the redundant case, the crank provides a strong constraint on how the arm can move. However, the oscillators do not need such a strong constraint in order to coordinate multiple degrees of freedom through mechanical coupling. A different task accomplished in this manner is passing a Slinky toy from hand to hand, as illustrated in figure 4-7. An independent oscillator is used to control each arm, only coupled by mechanical interactions with the Slinky toy itself. The oscillators quickly converge on an out of phase motion of the Slinky, as shown in figure 4-8. The coupling forces from the Slinky are small compared to the crank forces, but are still large enough to entrain the oscillators.

In all these examples, the oscillators are using the mechanical coupling though a physical structure to become coordinated with one another. This allows them to perform complicated tasks in a very simple manner. In the following section a simple model of this coupling is developed. The model shows that the behavior of the oscillators is to find the resonant mode of the mechanical system. Connecting the arm to the crank, or connecting the arms with a Slinky can thus be seen as altering the natural dynamics of the system so that the resonant mode is the movement required to successfully complete the task.

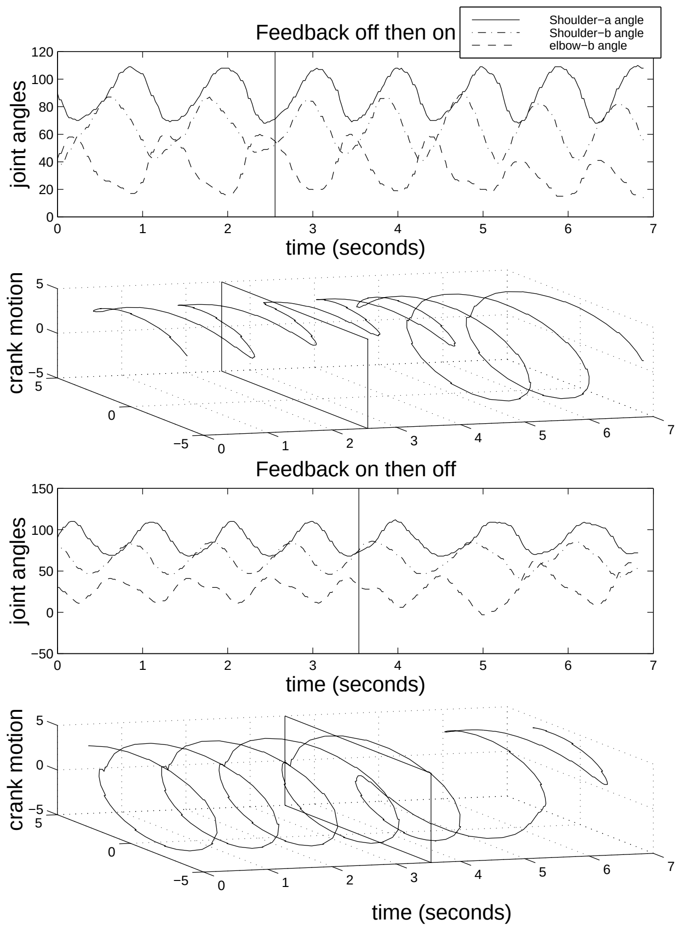

Figure 4-6: REAL Transients of crank turning with a redundant arm (the configuration shown in figure 4-5). Three degrees of freedom are shown here, for two shoulder joints and one elbow joint. The top two graphs show the joint angles, and the motion of the crank as the feedback is turned on, which occurs at the vertical line. The system has a short transient before finding the stable motion. The lower two plots show the same result, only this time the feedback is turned off at the vertical line. The system quickly falls out of coordination, and the crank stops being turned smoothly. The glitch in the crank trace is caused by the angle sensor wrapping round, not by a jerk in the motion.

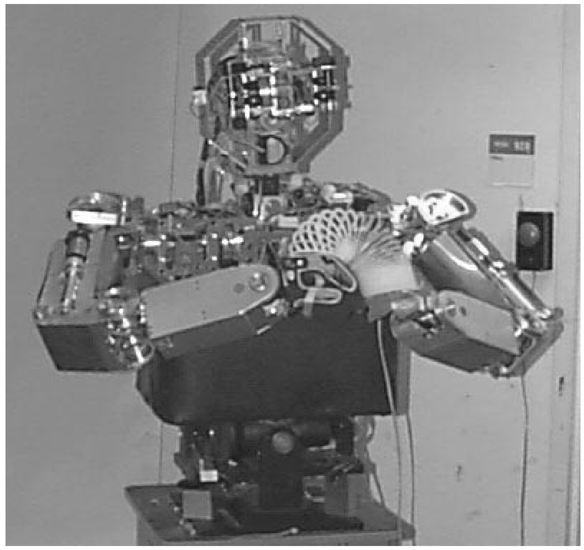

Figure 4-7: Picture of Cog passing the Slinky toy from hand to hand. The two elbow joints are used to move the hands up and down, where the coordination between the hands is given by the interaction between the oscillator dynamics and the coupled arm-slinky system.

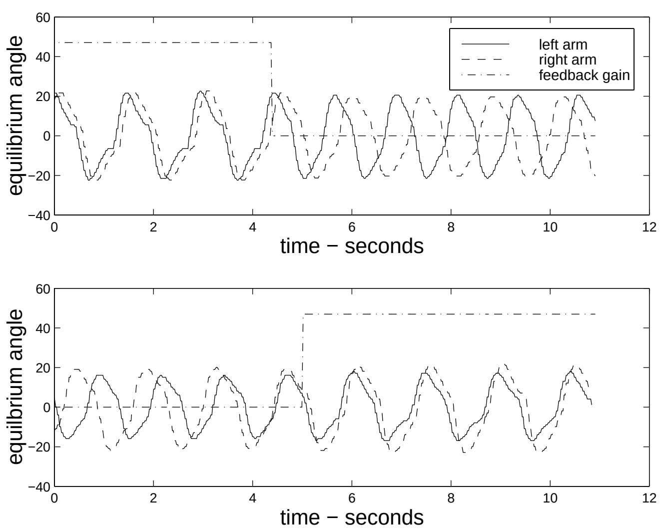

Figure 4-8: $\boxed{\text{REAL}}$ Two examples of Slinky operation. Both plots show the outputs from the oscillators as the torque feedback (dash-dot) is turned on and off. When the traces are in phase, the Slinky is moving in anti-phase. When the feedback is on, the two arms are coordinated and the outputs are synchronized, but when off, the oscillators are no longer synchronized. The only connection between the oscillators is through the physical structure of the Slinky.

4.2 Coupling model

The action of the mechanical coupling through the arm is to constrain the motion of each joint dependent on the motion of the other joints. Since the arm is compliant and in most configurations redundant, the coupling is not very stiff, i.e. there is some slop in the system. A simple approximation to this coupling is shown in figure 4-9. This shows two robot links represented as masses, with the joint level control appearing as a spring and damper connected to each mass. The coupling is included as a spring coupling the two masses, the stiffness of which can be varied to model the strength of the coupling. Using describing function analysis to represent the oscillators driving each mass extends the results in chapter 3 to this higher dimensional system.

In detail, the coupling model in figure 4-9 consists of two masses m_1, m_2 driven through springs k_1, k_2 and dampers c_1, c_2 by oscillators. The motion of each mass is coupled to the other by the coupling spring k_T.[2] The motion or angle of each mass is θ_1, θ_2, and the oscillator outputs are θ_{v1}, θ_{v2}.

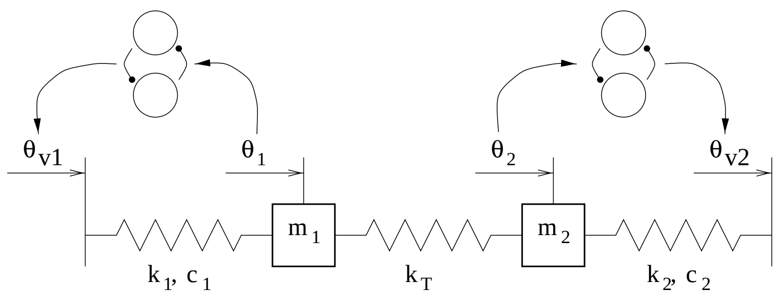

Figure 4-9: A simple model of coupling through the natural dynamics. The model consists of two masses driven by oscillators, connected by a coupling spring k_T.

The equations of motion for this system are

$$\begin{aligned} m_1\ddot{\theta}_1 + c_1\dot{\theta}_1 + (k_1 + k_T)\theta_1 - k_T\theta_2 &= k_1\theta_{v1} \\ m_2\ddot{\theta}_2 + c_2\dot{\theta}_2 - k_T\theta_1 + (k_2 + k_T)\theta_2 &= k_2\theta_{v2} \end{aligned} \tag{4.1}$$

This is a resonant mass-spring system, which has a free-vibration behavior when there is no driving input (i.e. $\theta_{v1} = \theta_{v2} = 0$). There are two resonant modes, at two different resonant frequencies. These can be determined by assuming solutions of the form $\Theta = Ae^{j\omega t}$, and solving the eigenvalue problem

$$\begin{pmatrix} (k_1 + k_T)/m_1 & -k_T/m_1 \\ -k_T/m_2 & (k_2 + k_T)/m_2 \end{pmatrix} \begin{pmatrix} \Theta_1 \\ \Theta_2 \end{pmatrix} = \omega^2 \begin{pmatrix} \Theta_1 \\ \Theta_2 \end{pmatrix} \tag{4.2}$$

for values of ω and ratios Θ_1/Θ_2.

When this system is driven by an oscillator, the behavior of the oscillator can be modeled using the describing function analysis developed in chapter 3. The oscillator behavior is expressed as a transfer function $N_i(j\omega, A)$, with a gain g_i and phase ϕ_i, evaluated over a range of frequencies and input amplitudes, i.e.

$$g_i e^{j\phi_i} = N_i(j\omega, A) \tag{4.3}$$

[2] In general the coupling should include a damper. Including the damper complicates the equations without changing their fundamental result so it was ignored.

Because the oscillator provides a driving force which is a function of the joint angles Θ, the effect of the oscillator is to turn the system from being a driven resonant system (4.1), to a freely vibrating system:

$$\begin{pmatrix} (k_1 + k_T + j\omega c_1 - k_1 g_1 e^{j\phi_1})/m_1 & -k_T/m_1 \\ -k_T/m_2 & (k_2 + k_T + j\omega c_2 - k_2 g_2 e^{j\phi_2})/m_2 \end{pmatrix} \begin{pmatrix} \Theta_1 \\ \Theta_2 \end{pmatrix} = \omega^2 \begin{pmatrix} \Theta_1 \\ \Theta_2 \end{pmatrix} \tag{4.4}$$

If this system has a steady state vibrating solution, then the solutions for ω must be real, since complex values of ω correspond to solutions which either decay or grow. This implies that the oscillator must cancel out the damping in the system, or in this case that the imaginary parts on the diagonals must be zero (Strang, 1993).

$$\omega c_1 - k_1 \mathrm{Im}[g_1 e^{\phi_1}] = \omega c_2 - k_2 \mathrm{Im}[g_2 e^{\phi_2}] = 0 \tag{4.5}$$

If the two oscillator driven systems are assumed to have the same damping factor ζ then this equation can be simplified. Writing $\omega_{ni} = \sqrt{k_i/m_i}$ and $2\zeta\omega_{ni} = c_i/m_i$ for each mass, the equation becomes

$$2\zeta\omega = \omega_{n1} g_1 \sin\phi_1 = \omega_{n2} g_2 \sin\phi_2 \tag{4.6}$$

This defines an important relation between the two oscillators, as well as a relation between the gain and phase of the individual oscillators and frequency. Because g_i and ϕ_i are both functions of frequency this equation can be solved numerically, fixing the frequency, and finding the value of A where

$$2\zeta\omega = \omega_{ni} \mathrm{Im}[N_i(j\omega, A)] \tag{4.7}$$

Figure 4-10 shows the solution to this equation for a typical choice of values for the masses and springs. The solution for each oscillator is indicated by the squares and stars on the plot. There are a range of solutions which vary in frequency, the extent of the solutions indicating the range of frequencies over which the oscillators can cancel out the damping, and produce steady state solutions.

The actual frequency of the motion depends on the solution for the eigenvectors of the complete system. When the imaginary parts have been removed, the problem reduces to

$$\begin{pmatrix} (k_1 + k_T - k_1 \mathrm{Re}[g_1 e^{j\phi_1}])/m_1 & -k_T/m_1 \\ -k_T/m_2 & (k_2 + k_T - k_2 \mathrm{Re}[g_2 e^{j\phi_2}])/m_2 \end{pmatrix} \begin{pmatrix} \Theta_1 \\ \Theta_2 \end{pmatrix} = \omega^2 \begin{pmatrix} \Theta_1 \\ \Theta_2 \end{pmatrix} \tag{4.8}$$

The effect of the oscillator is through the real part of its transfer function, $\mathrm{Re}[g_i e^{j\phi_i}] = g_i \cos\phi_i$. If the phase $\phi_i = 90°$, then this term is zero, and the equations reduce to the underlying mechanical system. This would imply that the oscillator driving this system simply removed the damping, but did not interfere with the shape of the motion. Unfortunately the phases are not exactly 90°, as show in figure 4-10. They lie in the range $90° - 160°$, which means that they affect the system. However, as the analysis below will show, they affect the frequency of the oscillation far more than the final mode shape.

The expression for the eigenfrequencies is obtained by solving (4.8) and is complicated:

$$\omega^2 = \frac{1}{2}\left[G_1 + G_2 + k_T\left(\frac{1}{m_1} + \frac{1}{m_2}\right) \pm \sqrt{(G_1 - G_2)^2 + 2k_T\left(\frac{1}{m_1} - \frac{1}{m_2}\right)(G_1 - G_2) + k_T^2\left(\frac{1}{m_1} + \frac{1}{m_2}\right)^2}\right] \tag{4.9}$$

where $G_i = (k_i/m_i)(1 - g_i \cos\phi_i)$. The values of g_i and ϕ_i are taken from the solutions to the damping constraint and are both functions of frequency. The equation can be solved numerically, with the

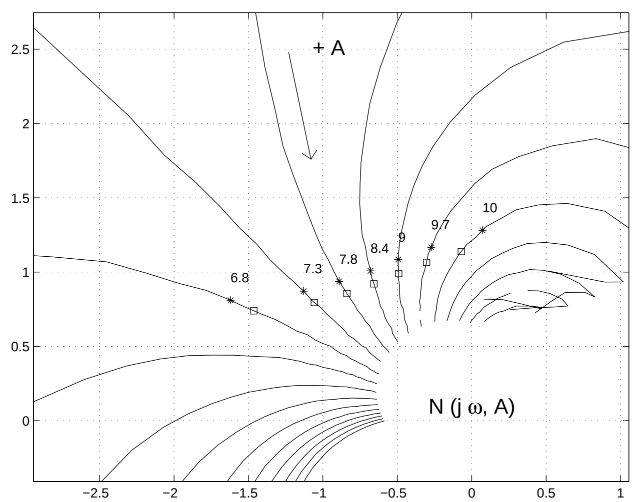

Figure 4-10: $\boxed{\text{SIM}}$ Figure showing solutions to the damping constraint (4.6). The plot shows $N(j\omega, A)$ in the complex plane, where the lines correspond to constant frequency, with increasing amplitude A as shown by the arrow. The squares and stars show the points where the damping in the system is zero ($*$ - mass 1, $\square$ - mass 2). The numbers show the frequencies of these solutions. The range of solutions indicates the range of frequencies over which the oscillators can drive the system. The solutions at the same frequency are close together, with similar amplitudes and phases. The phases vary from about 90° for $\omega = 10$ to near to 160° for $\omega = 6.8$. For this example, $k_1 = 30, m_1 = 1, c_1 = 4.65, k_2 = 25, m_2 = 1, c_2 = 3, k_T = 30$.

graphical interpretation of the solution shown in figure 4-11. This shows ω^2 plotted together with the right hand side of (4.9) evaluated at the damping solutions. In this case there are two possible solutions where the lines intersect, at $\omega = 7.4, 9.7$. The two solutions correspond to two different modes of the system motion, which can be calculated by evaluating the eigenvectors at those solution frequencies.

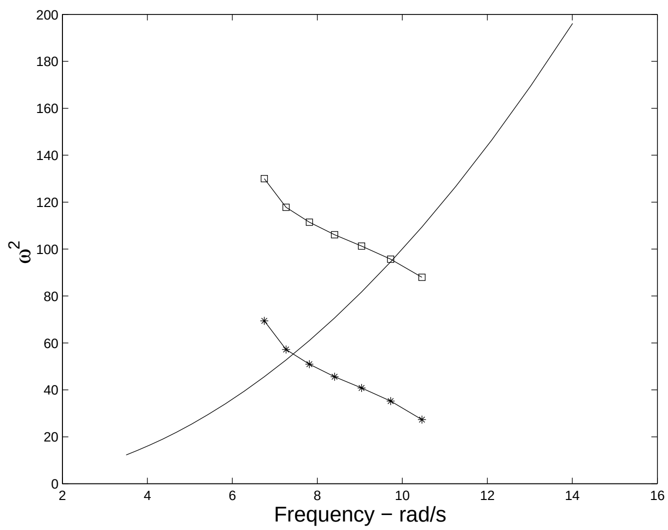

Figure 4-11: $\boxed{\text{SIM}}$ Figure showing solutions for the final system frequency. The plot shows ω^2 plotted together with the expression for the eigenvalues (equation (4.9)) evaluated at the oscillator solutions to the damping constraint. There are steady state solutions where the lines intersect, in this case there are two solutions at $\omega = 7.4, 9.7$. The plot shows that the oscillators produce at most as many solutions as there are modes of the underlying system, since there are only two possible intersections here.

The expression for the eigenvectors (4.9) carries little intuition, but can be simplified by considering the relationship between the damping constraint and the oscillator properties. The damping constraint (4.6) implies that the imaginary part of N multiplied by the local resonant frequency ω_{ni} is constant. The oscillators behavior is such that at constant frequency, the phase of N does not change greatly with input amplitude (see chapter 3, figure 3-7). This is also evident in figure 4-10, where the phases for the two solutions are approximately equal. Under this assumption,

$$\begin{aligned} G_1 - G_2 &= (\omega_{n1}^2 - \omega_{n2}^2) - (\omega_{n1}^2 g_1 \cos\phi_1 - \omega_{n2}^2 g_2 \cos\phi_2) \\ &\approx (\omega_{n1}^2 - \omega_{n2}^2) \end{aligned} \tag{4.10}$$

Assuming that this can be neglected compared to the other terms in the eigenvalue expression, (4.9) can be simplified, giving the two values of frequency ω:

$$\omega^2 \approx \begin{cases} (G_1 + G_2)/2 + k_T(\frac{1}{m_1} + \frac{1}{m_2}) \\ (G_1 + G_2)/2 \end{cases} \tag{4.11}$$

From which the eigenmodes of the system can be calculated. The ratio Θ_1/Θ_2 also has two values:

$$\Theta_1/\Theta_2 \approx \begin{cases} \frac{2k_T/m_1}{k_1/m_1 - k_2/m_2 - 2k_T/m_1} \\ \frac{2k_T/m_1}{k_1/m_1 - k_2/m_2 + 2k_T/m_2} \end{cases} \tag{4.12}$$

which is approximately the same as the resonant modes of the underlying mechanical system. Figure 4-12 shows the comparison between the modes of the mechanical system, and the modes found by the oscillator in this case.

Interestingly and importantly, the oscillator only finds one mode of the system. This is unlike the linear case, where the final solution is normally a superposition of the eigenmodes. One important constraint on the oscillator behavior is that it can only entrain over a limited range of frequencies. If the mode of the original system has a natural frequency which does not lie in this range, then the oscillator cannot have that mode as a periodic solution i.e. the lines in figure 4-11 will not intersect.

There are cases where there are two possible stable solutions, as in the example above. In that case the oscillator finds one or the other depending on initial conditions. Figure 4-14 shows two time traces of the transients finding either of the two modes for the example above. The reason for finding one solution is that the two modes correspond to different entrained frequencies for the oscillator. The oscillator can only output one frequency, (see chapter 3, figure 3-9), and thus cannot drive both modes simultaneously. This characteristic appears to be peculiar to the Matsuoka oscillator, as the Van der Pol oscillator (introduced in section 3.8) can drive two modes at once, as shown in figure 4-15. Driving two modes is undesirable for most applications.

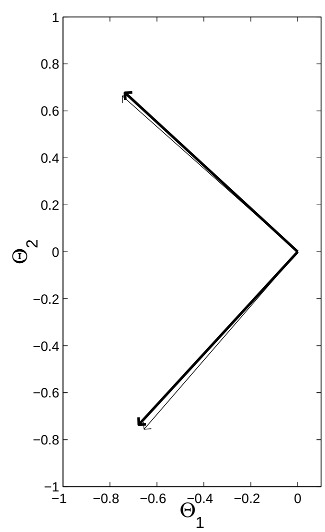

Figure 4-12: $\boxed{\text{SIM}}$ Plot showing eigenmodes of original system (thick arrow), and oscillator driven system (thin arrow). The mode is plotted as a vector in Θ_1, Θ_2 space. The arrows are close together, indicating that the oscillator solution is close to the resonant mode of the underlying mechanical system.

This behavior is robust, both to changes in oscillator and system parameters as shown in figure 4-13. It is also accurate. The oscillator drives relative to the motion of the system and accurately tracks the resonant mode. If the resonant mode of the system is the desired motion (as in the crank turning case described in the following section), then the oscillator behavior is automatically synchronized with the correct motion for the task.

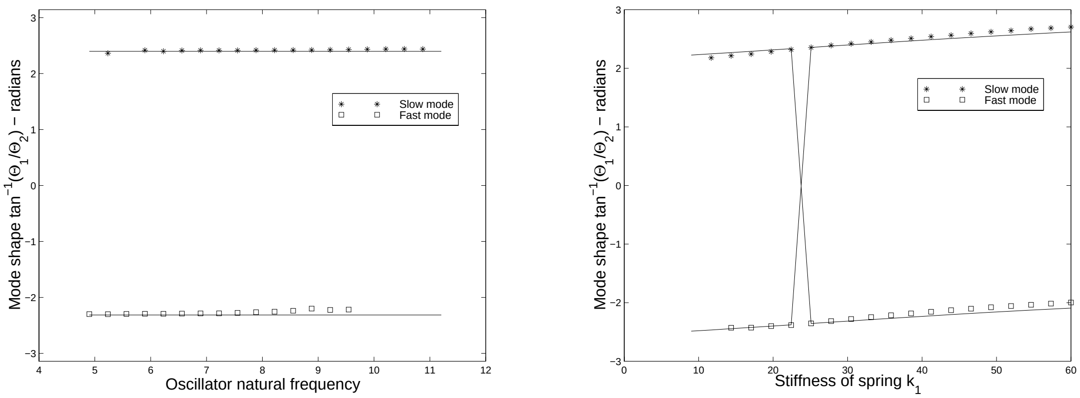

Figure 4-13: $\boxed{\text{SIM}}$ Plot showing robustness of oscillator to finding mode of system, under changing oscillator and system parameters. The y axis of the plots shows the angle of the mode in Θ_1, Θ_2 space, i.e. $\arctan(\Theta_1/\Theta_2)$. The left hand plot shows the effect of varying the natural frequency of the oscillator, with the lines indicating the underlying mechanical system modes. The accuracy of the oscillator is remarkable, given that the oscillator frequency doubles over the plot range. The right hand plot shows the effect of altering the stiffness of k_1, while keeping the other stiffness constant at $k_2 = 25$ Nm/rad. When k_1 is close to 25 Nm/rad the error in the modes is very low. As the stiffness gets bigger or smaller, the approximation $k_1/m_1 \approx k_2/m_2$ becomes less accurate, and the error gets bigger. However this is a minor effect. The robustness of the oscillator system is remarkable, given the change in stiffness of six times ($k_1 = 10 \leftrightarrow 60$ Nm/rad).

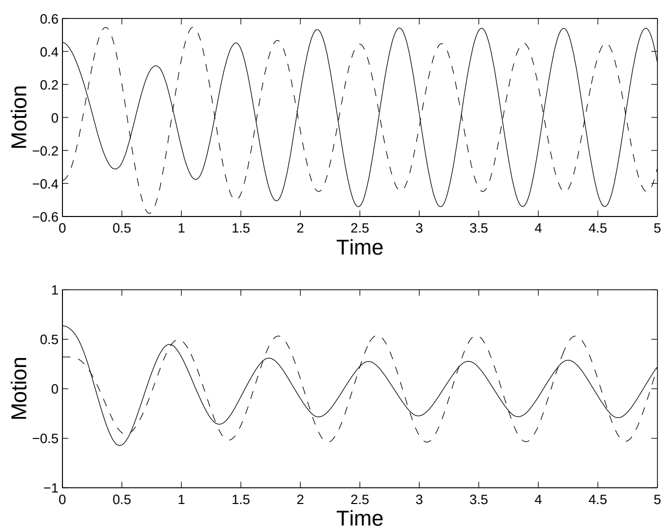

Figure 4-14: $\boxed{\text{SIM}}$ Plot showing the motion of mass 1 (solid) and mass 2 (dashed) of the oscillator driven system under two different initial conditions. The oscillator converges on one of the two modes of the system, with no mixing or superposition.

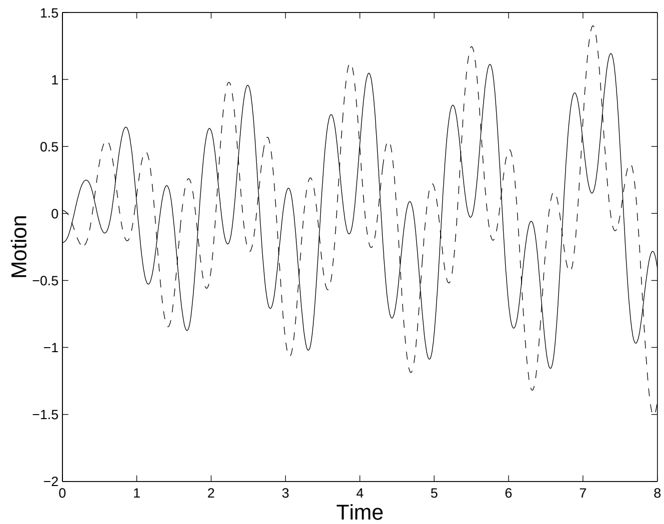

Figure 4-15: SIM Plot showing transient of the two mass system when a Van der Pol oscillator is used. This oscillator was described in section 3.8. The plot shows the motion of mass 1 (solid) and mass 2 (dashed) over time. Unlike the Matsuoka oscillator, this oscillator can give final periodic solutions which consist of a mixture of frequencies, as shown in the traces.

4.3 Local stability

The local stability of the oscillator limit cycle motion can be easily determined by examining the effect of amplitude changes on the damping in the system. At steady state, the oscillators exactly cancel the damping in the system, giving a constant amplitude oscillation. If an increase in amplitude results in positive (dissipative) damping, and a decrease in amplitude results in negative (excitatory) damping, then the limit cycle is stable.

The damping term is given by the diagonal elements of the system matrix:

$$c_{tot} = 2\zeta\omega - \omega_{ni}\mathrm{Im}[g_i e^{j\phi_i}] \tag{4.13}$$

Figure 4-16 shows $g_i e^{j\phi_i}$ plotted together with the line $j2\zeta\omega/\omega_{ni}$, for an example frequency $\omega = 7.8$. The steady state solution is marked with a box. If the amplitude of the oscillation increases, $\mathrm{Im}[g_i e^{j\phi_i}] < 2\zeta\omega/\omega_{ni}$, so $c_{tot} > 0$ which corresponds to positive damping, reducing the size of the oscillation. A decrease in amplitude has the opposite effect, confirming that the steady state oscillation is locally stable.

4.4 Summary of conclusions from the model

To conclude, the periodic solutions which exist for a set of oscillators driving a spring-mass system have the following characteristics

- The solutions are stable steady state solutions, with the oscillator canceling out the damping in the original system.
- The modes of the system are close to the eigenmodes of the original unactuated system, over a wide range of oscillator and system properties.

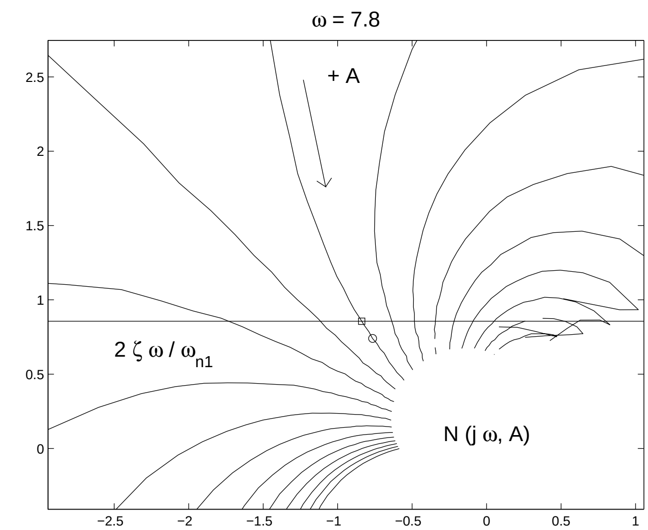

Figure 4-16: $\boxed{\text{SIM}}$ Figure showing $N(j\omega, A)$ and the line $j2\zeta\omega/\omega_{ni}$ to indicate the stability of the oscillator driven system. The damping term is given by $c_{tot} = 2\zeta\omega/\omega_{ni} - \text{Im}[g_i e^{j\phi_i}]$, which is zero at the steady state solution marked by a $\Box$. An increase in the amplitude of the motion moves the system to the point marked by the $\circ$, for which point the damping is positive because $2\zeta\omega/\omega_{ni} > \text{Im}[g_i e^{j\phi_i}]$. The positive damping will make the amplitude decrease. Similarly, a perturbation to lower amplitude results in negative damping, causing an increase in amplitude. The periodic solution is thus stable.

- The frequency of the final solution is not the eigenfrequency of the original mode, but is given by the interaction of the oscillator and system as defined by equations (4.6), (4.9).

The oscillator behavior of finding the resonant mode is useful because in some tasks such as crank turning the mode is exactly the desired motion for the task. The oscillators thus automatically find the correct coordination with the task. This complex property emerges from the interaction of the oscillators with the dynamics of the arm. No calibration, very little tuning, and no kinematic calculations are required to drive the arm along its resonant mode.

The following sections will show that the robot performance during both the crank turning and the Slinky toy tasks fit well with the simple model, providing evidence that exploiting the resonant mode is useful in practice.

4.5 Crank turning

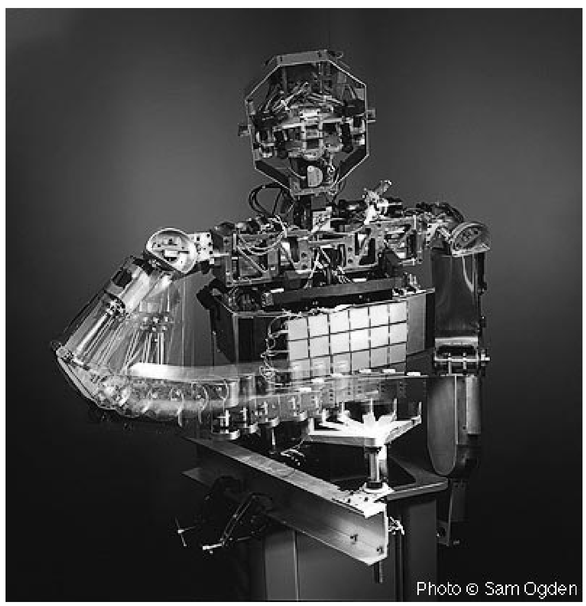

Figure 4-17: [
Picture of Cog turning a crank]Picture of Cog turning a crank. The robot is using two shoulder joints and two elbow joints to create the motion of the crank.

The crank turning behavior is a good example of the oscillators coordinated through the natural dynamics. The task is illustrated in figure 4-17. The crank turning can be understood in the context of the analysis of the previous chapter as a resonance of the springy arm around the constraint of the crank. The "springs" between the joints in this case are highly non-linear, but can be approximated by considering the solution of one mode of the system. This section compares data from the robot crank turning to the simple model developed in the previous section.

The full dynamics of crank turning are complicated and non-linear, but have the same general form as the full arm dynamics:

$$M(\Theta)\ddot{\Theta} + C(\Theta)\dot{\Theta} + K(\Theta)\Theta = K'\Theta_v \tag{4.14}$$

When this system is undergoing steady state oscillation it can be approximated a linear system, written as a set of eigenvalues and vectors. Transforming the variables $\Theta = Uq$, where U is the matrix of eigenmodes, and writing the effect of the oscillator as a diagonal matrix $G\exp(j\Phi)$, this equation can be written

$$U^T M U \ddot{q} + U^T C U \dot{q} + U^T K U q = U^T K' G e^{j\Phi} U q \tag{4.15}$$

Which looking at one mode u_i reduces to the single equation:

$$u_i^T M u_i \ddot{q}_i + u_i^T C u_i \dot{q}_i + u_i^T K u_i q_i = u_i^T K' G e^{j\Phi} u_i q_i \tag{4.16}$$

or approximately

$$\tilde{m}\ddot{q}_i + \tilde{c}\dot{q}_i + \tilde{k} q_i = u_i^T K' G e^{j\Phi} u_i q_i \tag{4.17}$$

The accuracy of this as a model of the crank turning problem can then be assessed by comparing real robot data to the predictions of the model.

The crank turning performance was measured for the robot in a configuration similar to that shown in figure 4-17, using four oscillators to actuate both shoulder, and both elbow joints. The oscillator time constants and the arm stiffness were varied to examine the behavior over a range of conditions. The frequency of the motion was calculated using a zero-crossing detector, and the amplitude and phase of the various joint motions and oscillator outputs was measured using a single frequency Fourier transform. The mode of the system u_i was directly calculated from the amplitudes and phases of the joint motions, and the gain of the oscillator directly measured by comparing joint motions and oscillator outputs. The stiffness and damping at each joint was also measured.

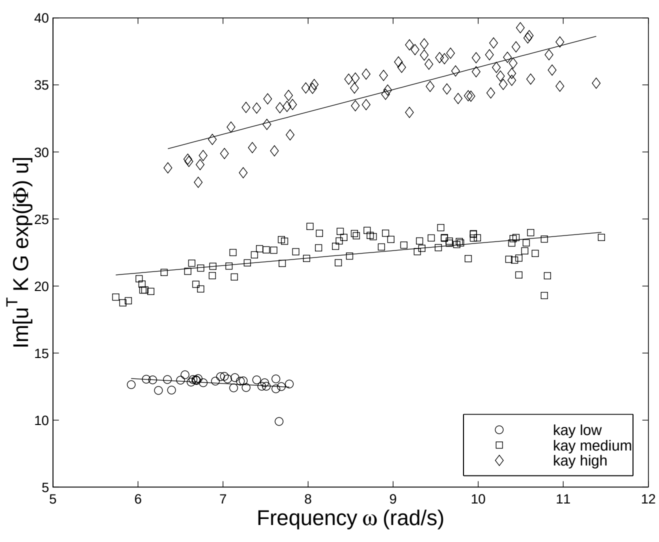

Figure 4-18: $\boxed{\text{REAL}}$ Plot of $\mathrm{Im}[u_i^T K' G e^{j\Phi} u_i]$ against ω for the crank turning. The crank turning involves four joints of the arm, for which the mode u_i is calculated from measured amplitude and phase data. The three lines correspond to different values of the arm stiffness (○ low, □ medium and ◇ high stiffness). The theory predicts that these points should lie on straight lines, the slopes of which are detailed in table 4.1.

The model of the crank turning predicts that the effect of the oscillator is to cancel out the damping in the system, or

$$\tilde{c}\omega \approx \mathrm{Im}[u_i^T K' G e^{j\Phi} u_i] \tag{4.18}$$

Figure 4-18 shows a plot of the imaginary part of the oscillator behavior versus ω. The data points were taken by measuring the system behavior as the natural frequency of the oscillatory was altered at three different values of arm stiffness (scaling the stiffness of all the arm joints in the ratio 1 : 2 : 3). The real damping at each joint was kept constant.

The theory predicts that this should be a straight line with slope proportional to $\tilde{c}$. The lines are straight, which is itself a good result given the simplicity of the model and the complexity of the arm motion. The slopes of the lines (listed in table 4.1) increase with stiffness, indicating that there is some coupling between the stiffness and damping through the arm dynamics. The abscissa are roughly constant which is as predicted.

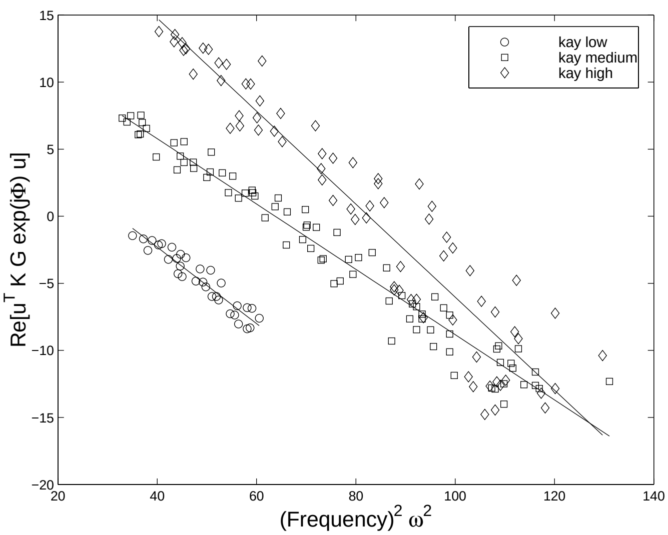

Figure 4-19: $\boxed{\text{REAL}}$ Plot of $\mathrm{Re}[u_i^T K' G e^{j\Phi} u_i]$ against ω^2. The theory predicts that these lines should be straight, with approximately constant slope. The lines have gradients $-0.28, -0.24, -0.35$ for increasing stiffness which are indeed roughly constant. The line for high stiffness is the most different from constant, and also the most noisy. The abscissa are at $9.08, 15.52, 28.64$ so roughly proportional to stiffness, as predicted by the model.

The theory also predicts that the real part of the oscillator should be inversely related to ω^2:

$$\tilde{k} - \tilde{m}\omega^2 \approx \mathrm{Re}[u_i^T K' G e^{j\Phi} u_i] \tag{4.19}$$

Figure 4-19 shows the plot for this situation. Again the straight lines are striking. The mass matrix of the system $\tilde{m}$ should be independent of the stiffness. The data supports this, with slopes which are roughly constant (see table 4.1). The abscissa reflect the effect of $\tilde{k}$ in the equation above, being roughly proportional to the stiffness.

The accurate fit of the crank turning data with the model shows that the model is a good description of the overall system. It also shows that the crank turning can be thought of as a resonant mode of the arm-crank system, which the oscillators are tuning into and exciting. This perhaps explains why the crank turning generalized so easily to multiple arms, the crank turning

	$\mathrm{Im}[u_i^T K' G e^{j\Phi} u_i]$				$\mathrm{Re}[u_i^T K' G e^{j\Phi} u_i]$			
	Slope		Abscissa		Slope		Abscissa	
kay	Value	Norm	Value	Norm	Value	Norm	Value	Norm
1	-0.34	**1**	15.13	**1**	-0.28	**1**	9.08	**1**
2	0.56	**-1.62**	17.63	**1.17**	-0.24	**0.86**	15.52	**1.71**
3	1.66	**-4.85**	19.67	**1.30**	-0.35	**1.22**	28.64	**3.15**

Table 4.1: $\boxed{\text{REAL}}$ Slopes and abscissa of the line fits in figures 4-18, 4-19. The raw values are shown in normal type, the normalized values in bold.

being the resonant mode of a larger system. It also suggests that the coupling through the Slinky toy also enforces a resonant mode of the two arm system.

The mode-finding property suggests that the oscillators would be suitable for other tasks where the resonance of the mass-spring system corresponds with the task. For example, other constrained tasks such as pumping a bicycle pump fall into this category. Methods to extend the oscillators to cases where the resonant mode of the system is not aligned with the task are described in chapter 5.

The oscillator behavior is useful because they automatically find the mode of the system without any extra computation, and they respond to the dynamics of the arm itself. The final solution is robust, because the oscillators are augmenting a natural motion of the arm.

The oscillator control is in fact more robust at high speeds, and does not work well at low speeds, which is the opposite of traditional robot control. For example, consider turning a crank using a stiff arm, with hybrid force/position control (Raibert and Craig, 1981). The arm would control force along the direction of the crank (and so exploit the physical crank to constrain the motion), and control position around the crank to move it. As the crank is turned faster and faster, the performance of both the position and force control will deteriorate as the dynamics of the arm become significant, requiring extra dynamical models. While intersegmental dynamics might change the exact structure of the crank-arm resonant mode, changing frequency will not change the fundamental structure of the dynamics. There will still be a resonant mode that the oscillators can find, and in any case the oscillators are responsive to the exact structure of the mode. By exploiting rather than canceling the arm dynamics, the oscillator system works well as the frequency increases.

4.6 Self-organization to find resonant mode

The oscillator system was always observed to find a rhythmic solution in the crank turning case. This corresponded to turning the crank all the way round over a wide set of parameters (see section 4.7), or to turning the crank part of the way round if the parameters where not set correctly. The coupling model predicts the existence of limit cycles and their local stability, but does not guarantee that the oscillators will find the solution. Unfortunately it is difficult to prove that the system will converge to the limit cycle (this is discussed further in chapter 6).

An intuitive explanation for the oscillator self-organizing behavior can be given in terms of the entrained state of the system. The oscillators start with some random phasing between one another, and by interacting with the crank settle on a solution where the phases differences between the oscillators are correct for the crank to be turned. The phases between the joints are varied by the oscillators falling in and out of entrainment with the arm.

At the steady state solution, all the joints need to move at the same frequency, with all the oscillators entrained. For the oscillator to be entrained, there needs to be a steady input, which would be given by the joint moving rhythmically. This means that there will only be a globally stable solution when all the oscillators have phases relative to one another so that they all get steady rhythmic signals from their joint angles. This situation corresponds to the crank being turned. If one of the oscillators does not get a steady input, it will become unentrained and its frequency will

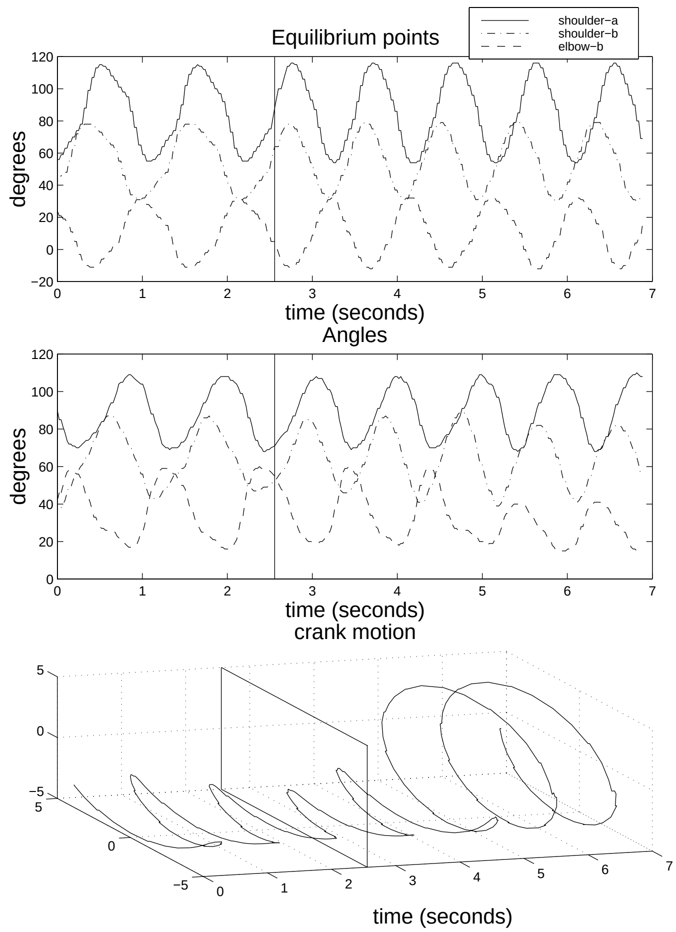

Figure 4-20: $\boxed{\text{REAL}}$ Transient of oscillator driven crank turning. The three plots show equilibrium points, joint angles and a schematic of the crank motion plotted against time. The feedback to the oscillators is controlled by the step trace, and the crank angle is indicated by the dashed line. When the feedback is turned on the oscillators at the different joints entrain to different frequencies causing the phases between the joints to change rapidly. When the stable turning phase is reached, the oscillators lock onto that phase, all the oscillators oscillate at the same frequency and the crank is turned stably.

change. The different frequency has the effect of rapidly varying the phases between the joints. When the phases between the joints becomes correct, the oscillators can stay entrained, and lock onto the crank motion. The process of falling into and out of entrainment thus allows the oscillators to change the phases between the joints, so finding the solution predicted by the describing function analysis.

Figure 4-20 shows a particularly long transient for the crank turning. When the feedback is switched on, the oscillators change their speed, which causes the phases between the different joints to vary. The elbow (dashed line) speeds up and then slows down when the system converges on the limit cycle motion.

4.7 Robustness

The oscillator solutions for crank turning are remarkably robust to choices of parameters. Crank turning can be achieved for a wide variety of different parameters, and a single set of parameters is appropriate for a wide range of system dynamic properties. The oscillator parameters can be divided into those which are extremely robust (values can be varied by factors of 3 or so without affecting performance), and those which are more sensitive (values can be varied by 15-20% without affecting performance).

The most robust parameters are the arm stiffness and inertia, oscillator time constants and oscillator feedback gains. Figure 4-21 shows the range of different arm stiffnesses and time constants which were tested on the robot. Both stiffness and time constants can be changed by factors of 3 without affecting performance. The feedback gain could be varied from values of 80 to 250 about a nominal value of 168. Figure 4-22 shows some results for two arm crank turning (the configuration shown in figure 4-4). The data shows the average turning speed and was taken by varying each parameter in turn while keeping the other parameters constant. The graphs show the robustness of the crank turning to these changes. In yet another experiment, 1 Kg masses were attached to both the upper and lower parts of the arm during crank turning, as shown in figure 4-23. These masses effectively doubled the inertia of each link so changing the arm natural frequency by approximately $\sqrt{2}$. Unfortunately no data was taken, but anecdotally the only effect was to reduce the speed of the crank turning slightly and not effect the coordination of the task.

Intuitively, the reason for this robustness is the entrainment properties of the oscillator. The final frequency of the crank depends on the arm stiffness and inertia as well as the oscillator frequency. Because the oscillator can entrain over a range of frequencies, the final motion can occur over a range of time constants and arm dynamic properties. The robustness to input gain is due to the oscillator properties; the oscillator output size and phase is for the most part independent of input size (see chapter 3).

The parameters which are more sensitive are the ones more tightly related to the resonant mode shape. These are the posture of the arm (about which it oscillates) and the amplitude of the joint motions (oscillator tonic parameter). These parameters have to be roughly correct: the crank turning will not work if all the joint amplitudes are zero, and the Slinky will not work if the hands are upside down. However, due to the compliance of the arm there is a significant range for these parameters which will perform the task.

Figure 4-24 shows the range of postures which gave reasonable turning for a two degree of freedom simulated arm (configuration similar to that shown in figure 4-2). The data was obtained by exhaustively testing postures near to a tuned solution. The posture of the shoulder and elbow joints can be independently varied by about 20% without affecting the crank turning. Figure 4-25 shows data from the real robot, again from the two arm crank configuration. The graphs plot the average turning speed as a function of parameter setting, with all other parameters kept constant. The posture of the shoulder has the most effect, as might be expected given its higher stiffness and it being the most powerful joint. Figure 4-26 shows the effect of varying the amplitudes at the

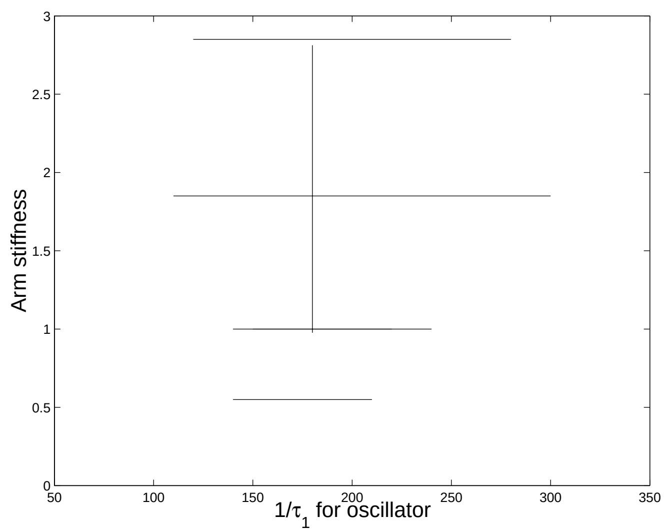

Figure 4-21: $\boxed{\text{REAL}}$ Plot showing robustness of the oscillator driven crank turning to changes in arm stiffness and oscillator time constants. The lines show the extent of crank turning solutions for various experiments, and thus are samples of the underlying range of parameters possible. The ranges of working parameters was found by altering both the arm stiffness (by changing each joints stiffness by the ratio indicated from a nominal stiffness), and the oscillator natural frequency (changing τ_1 for all the oscillators). All these lines were taken with the same input scale. The range of robustness is clear, with both parameters changing by factors of 3, while still performing crank turning.

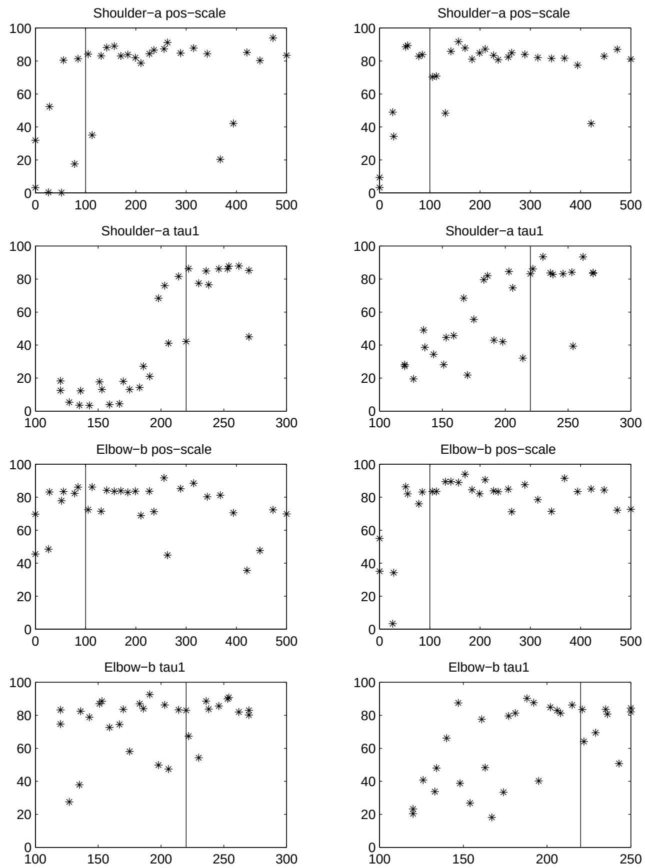

Figure 4-22: $\boxed{\text{REAL}}$ The graphs show the average crank turning speed (in revs per minute) over four seconds starting from rest for two arm crank turning (the configuration shown in figure 4-4). Each graph shows the effect of varying one parameter while keeping all the others at their default values (indicated by vertical lines). The left hand column refers to changes in the left arm, and the right hand column to right arm changes. The inputs gains (marked pos-scale on figure titles) can be varied greatly without affecting performance. The time constants (marked tau1) also show some variation, requiring a minimum value for crank turning to work. The data shows the effect of varying the time constant at one oscillator while keeping all the other parameters constant, which is why the data is less robust than that in figure 4-21 where all the time constants were varied together. The ability of the oscillator to entrain over a range of frequencies is illustrated by insensitivity to time constants especially at higher values. The data was taken over a short period of time so part of the noise in the data is due to slow transients, rather than necessarily being a consequence of poor turning solutions.

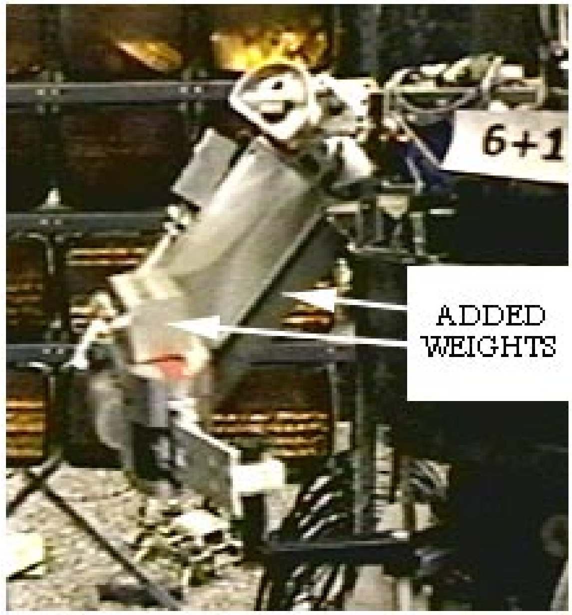

Figure 4-23: REAL To demonstrate robustness of the oscillator system, it was used with two 1 Kg masses attached to the upper and lower parts of the arm. These masses effectively double the inertia of the arm links. Their effect on the oscillator control was to make the system turn the crank slower, but did not disrupt the crank motion. In this picture all six degrees of freedom of the arm were used to turn the crank.

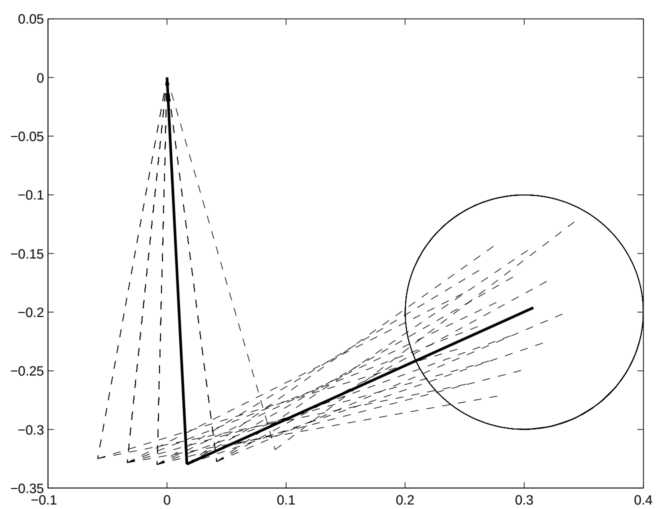

Figure 4-24: SIM The graph shows the range of postures which give good crank turning for a two degree of freedom simulated arm. The turning was measured by simulating the system and recording those postures which gave 70% of the maximum average speed over a four second transient. The plot gives a good indication of the variation in posture that can be tolerated while still giving good turning. The solid line shows the posture with the highest speed.

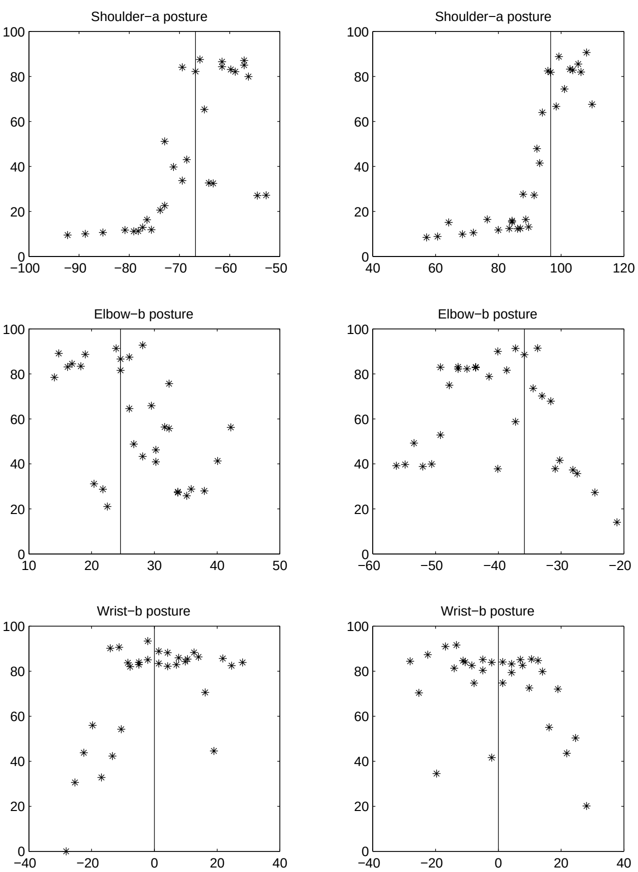

Figure 4-25: REAL The graphs show the average crank turning speed (in revs per minute) over four seconds starting from rest for two arm crank turning (the configuration shown in figure 4-4). Each graph shows the effect of varying the arm posture while keeping all the others at their default values (indicated by vertical lines). The postures are expressed in degrees. The left hand graphs are for changes to the left arm, and vice versa. The graphs indicate that the range of postures for each joint for successful crank turning is about $10° - 20°$. The data was taken over a short period of time so part of the noise in the data is due to slow transients, rather than necessarily being a consequence of poor turning solutions.

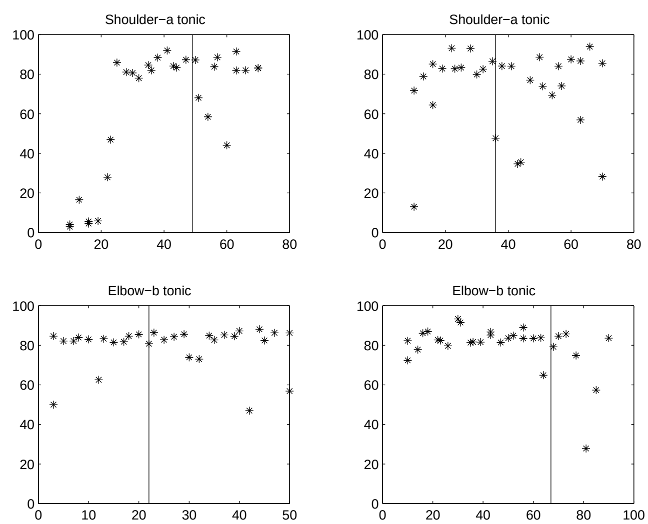

Figure 4-26: $\boxed{\text{REAL}}$ The graphs show the average crank turning speed (in revs per minute) over four seconds starting from rest for two arm crank turning (the configuration shown in figure 4-4). Each graph shows the effect of varying the oscillator output amplitudes while keeping all the others at their default values (indicated by vertical lines). The left graphs refer to changes in the left arm and vice versa. The only parameter that appears to be sensitive is the shoulder-a amplitude (tonic) of the left arm. Once this parameter is large enough, the crank turning is possible for a range of parameters. The system works with large values of these parameters by turning the crank more violently, the oscillators still finding the correct coordination.